ENGINEERING DEVELOPMENT OF SLURRY BUBBLE COLUMN REACTOR (SBCR) TECHNOLOGY

Quarterly Technical Progress Report No. 21
For the Period 1 April – 30 June 2000

FINAL

Contractor
AIR PRODUCTS AND CHEMICALS, INC.
7201 Hamilton Blvd.
Allentown, PA 18195-1501

Bernard A. Toseland, Ph.D.
Program Manager and Principal Investigator

Robert M. Kornosky
Contracting Officer's Representative

Prepared for the United States Department of Energy
Under Cooperative Agreement No. DE-FC22-95PC95051
Contract Period: 3 April 1995 – 31 March 2002

ENGINEERING DEVELOPMENT OF SLURRY BUBBLE COLUMN REACTOR (SBCR) TECHNOLOGY

Quarterly Technical Progress Report No. 21
For the Period 1 April – 30 June 2000

Project Objectives

The major technical objectives of this program are threefold: 1) to develop the design tools and a fundamental understanding of the fluid dynamics of a slurry bubble column reactor to maximize reactor productivity, 2) to develop the mathematical reactor design models and gain an understanding of the hydrodynamic fundamentals under industrially relevant process conditions, and 3) to develop an understanding of the hydrodynamics and their interaction with the chemistries occurring in the bubble column reactor. Successful completion of these objectives will permit more efficient usage of the reactor column and tighter design criteria, increase overall reactor efficiency, and ensure a design that leads to stable reactor behavior when scaling up to large diameter reactors.

Iowa State University

The report from Iowa State University for the period follows. Note that this is Iowa State's second contribution to this series of quarterlies.

ENGINEERING DEVELOPMENT OF SLURRY BUBBLE COLUMN REACTOR (SBCR) TECHNOLOGY

Investigation of Chemical Source Term Closures For Multiphase Turbulent Reacting Flows

Second Quarterly Report
for
April 1 - June 30, 2000
(Budget Year 1 – 2nd Quarter)

Iowa State University

Objectives for First Year

- ***First Quarter****:* Review existing CFD models for gas-liquid flows and determine the importance of various momentum exchange terms. Begin simulations and evaluate the feasibility of using various multiphase CFD codes (e.g., Fluent, MFIX, CFDLIB).
- ***Second Quarter****:* Compare two-dimensional (2D), time-dependent versus steady-state simulations for gas-liquid flows and validate simulations with available experimental data. Examine scaleup issues associated with hydrodynamics in large-diameter columns using multiphase simulations with periodic boundary conditions.
- ***Third Quarter****:* Continue investigation of hydrodynamic issues. Work on parallel implementation of CFD code on multiprocessor machines using MPI. Begin review of existing multiphase scalar (e.g., energy and chemical species) transport models.
- ***Fourth Quarter:*** Begin implementation of the various inter-phase scalar transfer models in multiphase CFD simulations and compare with available experimental data. Study grid dependence of the CFD solutions, and develop strategies for eliminating it.

HIGHLIGHTS FOR THE QUARTER

- Ported CFDLIB (serial version) to SUN Ultra 10 and SGi Origin 2000.
- Learned to employ CFDLIB by running tutorials and studying in detail the structure of the code.
- Completed CFDLIB simulations for cases done previously with Fluent.
- Continued to meet regularly with the multiphase research group at Ames Laboratory to develop a research initiative focused on multiphase closures.

SUMMARY OF PROGRESS

As discussed in our last quarterly report, we are currently investigating uncertainties in the hydrodynamic models of two-phase flow. In particular, the effects of grid size, time step, and the formulation of the two-phase Eulerian-Eulerian models are all being studied. In order to address these questions, we are continuing with a series of CFD simulations of two-phase flow with periodic boundary conditions to isolate the flow dynamics inherent in the model equations in the absence of wall effects. Furthermore, the computational grid chosen is much finer than is usually reported in the literature in order to resolve fully all terms in the model equations.

As reported in our previous quarterly report, our initial simulations were carried out with a commercial CFD code (Fluent 4). However, even for 2D bubble columns, we could not carry out the simulations beyond 2-3 seconds due to numerical instabilities. Furthermore, Fluent required a large amount of time for convergence at each time step largely due to the implicit formulation and the computational overhead associated with the graphics interface. In order to reduce the turnaround time, we have also tried the parallel implementation of Fluent on the ISU Origin 2000. However, in part because of the numerical instability, we did not obtain satisfactory scaleup when the number of processors exceeded two or three. Finally, it must be noted that Fluent has the inherent inflexibility of not giving us direct access to the model equations contained in the source code. Since we are interested in testing new closures, we find this limitation to be unacceptable.

Due to the above-mentioned reasons, we are now using CFDLIB (FORTRAN LIBRARY FOR CFD from LOS ALAMOS NATIONAL LABORATORY) for multiphase simulation. CFDLIB has no graphics overhead, provides direct access to the source code, and is more robust than Fluent because of its explicit formulation. Our tests with CFDLIB running on a single-processor workstation have confirmed the positive attributes (e.g., fast convergence, stability over a wide range of grid sizes) that have been reported in the literature. Furthermore, Padial, Kashiwa, and Kothe (1994) have reported linear speedup for CFDLIB on a Cray T3D using the PVM communication protocol. So far, we have run CFDLIB successfully in serial mode, and are working with the ISU high-performance computing consultants to port a parallel version to the ISU Origin 2000.

SELECTED RESULTS

Example 1: Comparison between Fluent 4.4 and CFDLIB for simulation of a 2D bubble column.

Physical Dimensions: 2.6 cm (width) by 9.6 cm (height)

The column was initially filled with water to a height of 8 cm. The grid spacing was set at 0.1 cm, and the bubble diameter was 5 mm. Only the drag and virtual mass forces were taken into account. In all simulations, it was found that CFDLIB converged much faster than Fluent. For example, 6 hrs of CPU time using CFDLIB on a single processor of the Origin 2000 were required to simulate 2.43 seconds, whereas with Fluent 4.4, 24 hrs were required to run the same simulation. More important, CFDLIB continued to run for longer times, whereas Fluent would not converge beyond about 3 seconds. Furthermore, due to the explicit formulation, CFDLIB

code was overall much more robust than Fluent 4.4. For example, Fluent required extensive tuning of the under-relaxation factors and time-step in order to have the simulation converge. This process required frequent operator intervention, which greatly limited our ability to run large simulations. On the other hand, CFDLIB automatically adjusted the time step to optimize convergence without operator intervention.

The parallel version of CFDLIB will be implemented in the next quarter. We will then attempt to simulate larger 3D bubble columns, and to evaluate the importance of various momentum closure terms.

Example 2: Two-dimensional, time-dependent simulation with symmetric wall boundary conditions for air-water system.

Description of problem
Physical dimension: 0.078 m by 0.39 m
Grid size: 50 (width) by 250 (height)
Bubble diameter: 2.6 mm.
Air inlet velocity: 0.01 m/sec

Only the drag force and virtual mass terms were enabled in the laminar two-phase flow model. The CFDLIB simulation required 14 hours on a SUN ULTRA 10 to simulate for 1.74 seconds. The average time-step used by CFDLIB was $\sim 10^{-4}$ seconds. Figures 1.1, 1.2 and 1.3 show the water volume fraction, water velocity field, and air velocity field, respectively, after 1.74 seconds. Note that the symmetric boundary conditions eliminate transport (momentum, mass) through the walls. The air phase thus rises nearly uniformly through the simulation domain. On the other hand, the water phase has zero mean velocity, so that the momentum it receives from the gas phase generates vorticity, which is eventually dissipated at small scales.

We are currently exploring the dependency of the turbulent structures generated in wide columns on the grid resolution. These results will be presented at the CFD in Chemical Reaction Engineering conference in Quebec in August 2000.

References

Padial, N. T, B. A. Kashiwa, and D. B. Kothe, "Status of CFDLIB performance tests on the T3D," Cray User Conference, CEA/CEL-V, France, October 10-14, 1994.

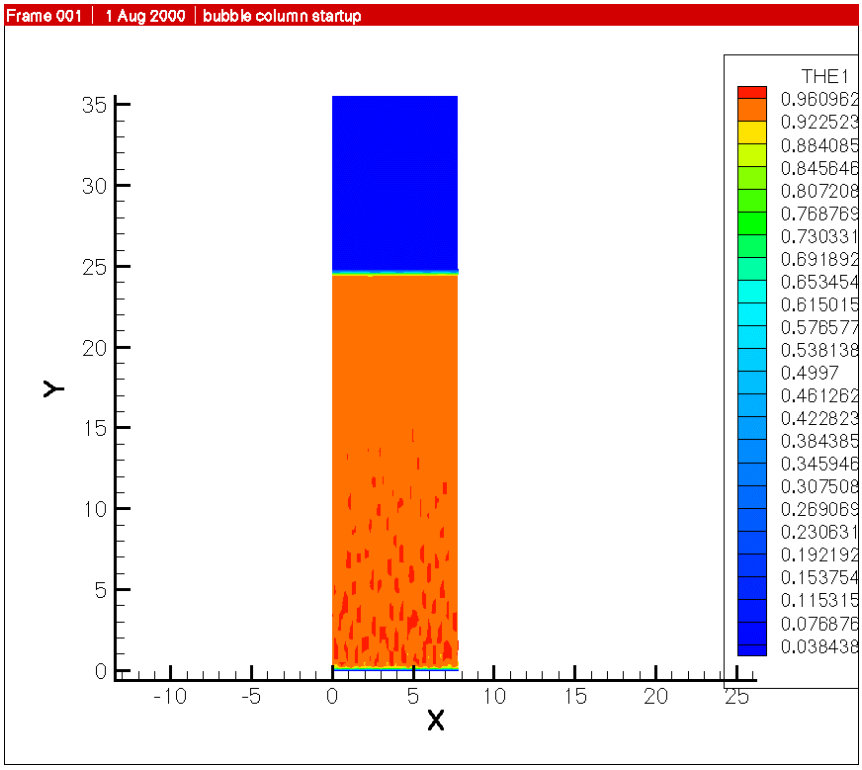

Figure 1.1 Water Volume Fraction at 1.74 Seconds

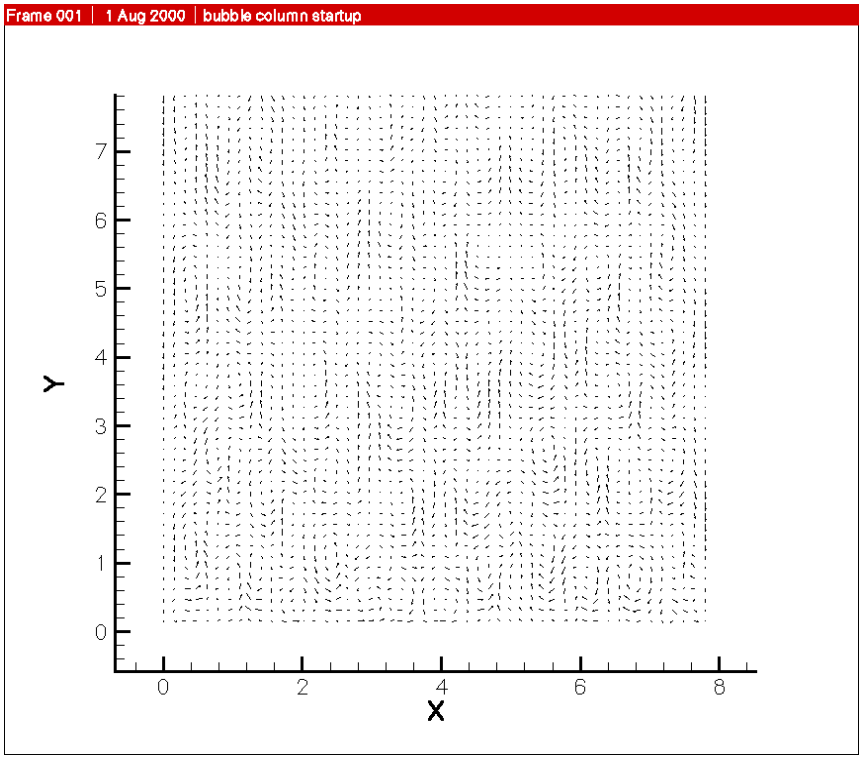

Figure 1.2 Water Velocity Field at 1.74 Seconds

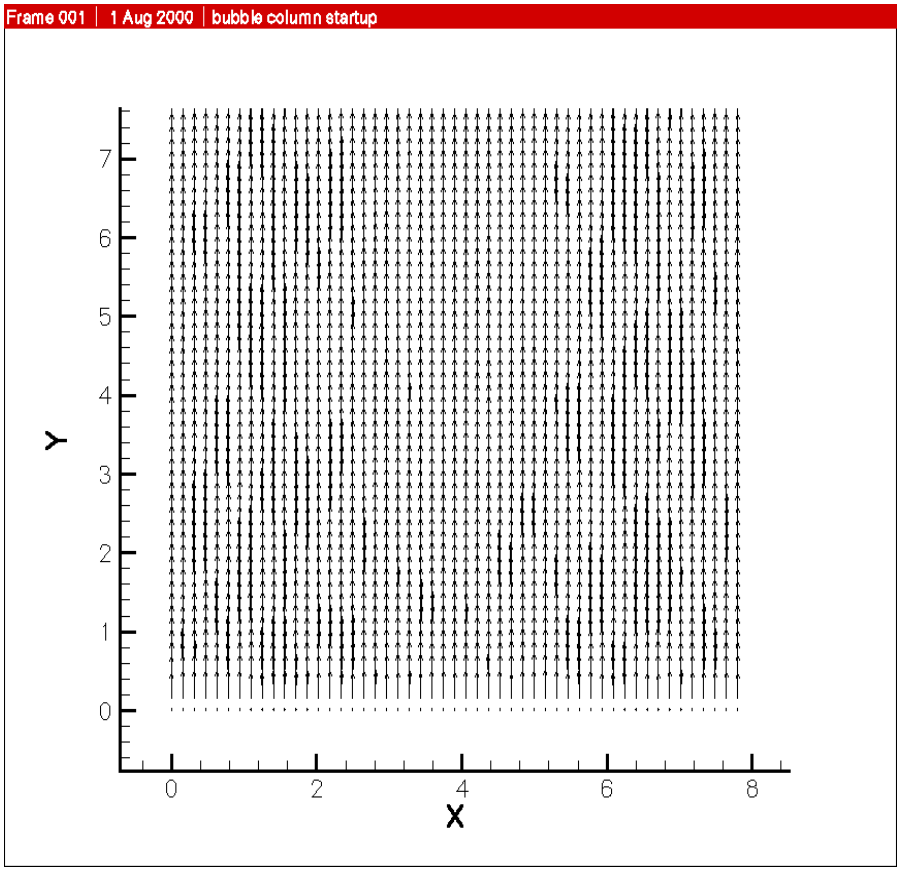

Figure 1.3 Air Velocity Field at 1.74 Seconds

The Ohio State University

The report from Ohio State University for the period follows.

INTRINSIC FLOW BEHAVIOR IN A SLURRY BUBBLE COLUMN UNDER HIGH PRESSURE AND HIGH TEMPERATURE CONDITIONS

Quarter Report

(**Reporting Period:** April 1 to June 30, 2000)

Heat Transfer Characteristics in Slurry Bubble Columns at Elevated Pressures and Temperatures

Highlights

- The heat transfer behavior between an immersed heating surface and the surrounding gas-liquid-solid medium was investigated experimentally and analytically at elevated pressures and temperatures.

- Effects of gas velocity, solids concentration, pressure and temperature on the heat transfer coefficient were examined. It was found that the heat transfer coefficient increases as the gas velocity increases then levels off.

- The heat transfer coefficient in slurry bubble columns decreases significantly with an increase in system pressure. The effect of pressure on the heat transfer coefficient is attributed to the variations in liquid properties, bubble size and gas holdup with pressure.

- Both the increased liquid viscosity and the decreased bubble size with increasing pressure result in a decrease in heat transfer coefficient. An increase in gas holdup with increasing pressure increases the surface renewal rate and thus the heat transfer rate. The combination of these effects gives rise to the overall effect of pressure on heat transfer behavior in gas-liquid-solid systems.

- The addition of particles to the liquid phase enhances heat transfer substantially, and the heat transfer coefficient increases significantly with increasing temperature. The effect of temperature on the heat transfer coefficient is mainly determined by the change in liquid viscosity.

- By considering the effect of gas holdup on heat transfer behavior, we propose an empirical correlation to predict the heat transfer coefficient in slurry bubble columns under high-pressure conditions.

- The consecutive film and surface renewal model is capable of describing the heat transfer characteristics in slurry bubble columns at high pressures. The major heat transfer resistance is within a fluid film surrounding the heating surface.

Work Conducted

Experimental Study

Effect of Gas Velocity

Figure 1 shows the variation of heat transfer coefficient with gas velocity and pressure in slurry bubble columns. The heat transfer coefficient increases as the gas velocity increases and then levels off. Many studies conducted under ambient conditions have also shown a similar trend of gas velocity effect (Deckwer, 1980; Saxena et al., 1990). According to the theory of isotropic turbulence, the heat transfer rate is controlled by the energy dissipation induced by micro-scale eddies. At high gas velocities, the gas flow in the slurry bubble column is in the form of large bubbles. The large bubbles do not significantly affect the energy transfer at the micro-scale level; instead they induce an enhanced liquid internal circulation (Deckwer, 1980). The internal circulation does not improve the heat transfer coefficient appreciably, and hence a leveling off of the heat transfer coefficients occurs at high gas velocities.

Effect of Pressure

Figure 1 also shows that the heat transfer coefficient decreases significantly with an increase in pressure. This behavior can be attributed to the variations in physical properties of the liquid phase, bubble size and gas holdup with pressure. Since the heat transfer behavior is closely associated with macroscopic flow structures and microscopic flow characteristics, a variation in pressure, which alters the hydrodynamics, would yield a significant effect on the heat transfer behavior in the slurry system. Previous studies on heat transfer in gas-liquid and gas-liquid-solid systems indicated that an increase in the liquid viscosity decreases the heat transfer coefficient (Kato et al., 1981; Kang et al., 1985; Deckwer, 1980; Kumar and Fan, 1994). The decrease in heat transfer coefficient with increasing liquid viscosity is possibly due to the fact that the thickness of the laminar sublayer in turbulent flow increases with liquid viscosity. Since the liquid viscosity increases with pressure, increased pressure would decrease the heat transfer coefficient due to the variation in liquid viscosity. Other physical properties of the liquid, such as density, thermal conductivity and heat capacity, are less affected by pressure (Reid et al., 1977).

The heat transfer coefficient is also affected by the bubble characteristics and hydrodynamics such as bubble size and gas holdup. Kumar et al. (1992) found that the injection of a single bubble into liquids or liquid-solid suspensions enhances the heat transfer rate via bubble wake. Since wake size is proportional to bubble size, a larger bubble would have a larger wake and stronger vortices associated with the wake, thereby enhancing the rate of heat transfer. Since the bubble size decreases with increasing pressure, the pressure would have a negative effect on the heat transfer coefficient. Gas holdup can also affect heat transfer behavior. Under high gas holdup conditions, the turbulence induced by the intense bubble-wake, bubble-bubble, and bubble-surface interactions would augment the rate of heat transfer surface renewal. Since the gas holdup and the bubble number density increase significantly with pressure, the frequency of

bubble passage over the heating surface increases with pressure, and thus increases the heat transfer rate. The combination of above effects gives rise to the overall effect of pressure on the heat transfer rate.

Effect of Solids Concentration

The effect of particles on the heat transfer coefficient under ambient pressure and elevated pressure (P=4.2 MPa) is shown in Figure 2. For the present system, the addition of particles to the liquid greatly increases the heat transfer coefficient. This behavior can be explained by the larger bubble size in the slurry system compared to the pure liquid. Luo et al. (1999) measured the bubble size distribution in a slurry bubble column by using an optic fiber probe and found that the mean bubble size increases significantly with an increase in solids concentration, especially under ambient pressure. Thus, the heat transfer coefficient increases significantly with an increase in solids concentration. The extent to which solids concentration affects the heat transfer coefficient differs at different pressures. The effect of solids concentration on the heat transfer coefficient at ambient pressure is more profound than that at high pressure, since the bubble size is relatively large and the effect of solids concentration on bubble size is more remarkable at ambient pressure (Luo et al., 1999). At high pressures, the heat transfer coefficient in the three-phase system is higher than that in the two-phase system, while the difference in the heat transfer coefficients for solids concentrations of 20% and 35% appears to be insignificant. The reason is that the bubble size does not vary significantly with a further increase in solids concentration at high pressures (Luo et al., 1999).

Effect of Temperature

The effect of temperature on the heat transfer coefficient is shown in Figure 3. For all the pressures considered, when the temperature increases, the heat transfer coefficient increases significantly. This phenomenon can be explained by the significant decrease in liquid viscosity with increasing temperature. Among the three factors that affect the heat transfer rate, i.e., liquid viscosity, bubble size and gas holdup, liquid viscosity is the one most affected by temperature. Liquid viscosity decreases significantly with increasing temperature, which results in an increase in the heat transfer coefficient. For example, at a pressure of 4.2 MPa, the liquid viscosity decreases from 0.024 Pa·s to 0.0053 Pa·s, i.e., a 78% decrease as the temperature increases from 35 to 81^{o}C. Based on the correlation proposed by Deckwer (1980), the heat transfer coefficient is proportional to the -0.25 power of the liquid viscosity in gas-liquid systems. Therefore, the 78% decrease in liquid viscosity would result in a 46% increase in heat transfer coefficient. From the experimental data shown in Figure 3(a), at a gas velocity of 10 cm/s, the heat transfer coefficient increases from 514 to 676 w/m^2·k, i.e., a 32% increase as the temperature increases from 35 to 81^{o}C. Thus, the change in liquid viscosity is the determining factor for the effect of temperature on the heat transfer coefficient in the system being studied.

Heat Transfer Correlation: Among various factors that affect the heat transfer coefficient from an immersed surface to the surrounding medium in bubble columns, the most important are liquid properties (ρ_l, μ_l, k_l and C_{pl}), operating conditions (u_g), and hydrodynamics (d_b *and* ε_g). Based on the Higbie surface renewal model and the Kolmogoroff theory of isotropic turbulence, Deckwer (1980) proposed the following form of semi-theoretical correlation to predict the heat transfer coefficient in bubble columns:

$$St = c\left(\mathrm{ReFrPr}^{a}\right)^{b} \tag{1}$$

where *St, Re, Fr* and *Pr* are, respectively, Stanton, Reynolds, Froude and Prandtl numbers based on the liquid properties, and *a*, *b* and *c* are constants obtained by fitting the experimental data. Based on the semi-theoretical analysis, Deckwer (1980) found that *a*, *b* and *c* are equal to 2, -0.25 and 0.1, respectively. Other researchers (Kast, 1962; Shaykhutdinov et al., 1971; Hart, 1976; Steiff and Weinspach, 1978) also used this form of correlation to represent their heat transfer results and found that the values of parameters *a*, *b* and *c* are in the ranges of 1.9 ~ 2.5, -0.27 ~ -0.22, and 0.1 ~ 0.14, respectively, as summarized by Deckwer (1980). By assuming that the liquid-solid suspension is a homogeneous phase, Deckwer et al. (1980) found that Eq. (1) can also be used in a slurry system if the physicochemical properties of the slurry can be estimated from the individual phases. Equation (1) is only perceived to be applicable for ambient pressure, since this correlation was obtained in systems in which gas holdup is not affected by pressure. However, for systems in which pressure has a significant influence on the hydrodynamics, the pressure effect on the heat transfer coefficient should be considered in the correlation. For the system in the present study, the experimental results indicate that pressure has a significant effect on heat transfer behavior in both bubble columns and slurry bubble columns. Therefore, in order to extend Eq. (1) to the high-pressure conditions, it is necessary to include the terms that account for the effect of pressure in the correlation. Studies in the literature have indicated that the heat transfer coefficient in bubble columns is influenced by gas holdup (Zehner, 1986; Magiliotou et al., 1988), and since gas holdup strongly depends on system pressure (Luo et al., 1999), including the gas holdup term in the correlation would account for the pressure effect on the heat transfer coefficient. The analytical model discussed in the next section reveals that h_w may be related to $(1-\varepsilon_g)/\varepsilon_g$, i.e.:

$$h_w \propto \left(\frac{1-\varepsilon_g}{\varepsilon_g}\right)^{\alpha}. \tag{2}$$

Based on Eq. (1) and considering the effect of gas holdup on the heat transfer coefficient, the following correlation is proposed to quantify the heat transfer coefficient in a slurry bubble column at elevated pressures:

$$St_m = c\left[\left(\mathrm{Re}_m\, Fr\, \mathrm{Pr}_m{}^{a}\right)\left(\frac{\varepsilon_g}{1-\varepsilon_g}\right)\right]^{b}. \tag{3}$$

The constants *a, b* and *c* are obtained by fitting the experimental data. For the present system, *a, b* and *c* are found to be 1.87, -0.22 and 0.037, respectively.

To use Eq. (3), the density and the heat capacity of the suspension can be evaluated by

$$\rho_m = \rho_l\left(1-\varepsilon_s\right) + \rho_s\varepsilon_s \tag{4}$$

$$C_{pm} = C_{pl}(1-\omega_s) + C_{ps}\omega_s \tag{5}$$

where ω_s represents the weight fraction of the solid phase. Basing his work on the electrical analogy for liquid-solid suspensions, Tareef (1940) proposed the following equation to calculate the thermal conductivity of the suspension:

$$k_m = k_l \frac{2k_l + k_s - 2\varepsilon_s(k_l - k_s)}{2k_l + k_s + \varepsilon_s(k_l - k_s)}. \tag{6}$$

The suspension viscosity of the present system is calculated based on the correlation proposed by Luo et al. (1997) as follows:

$$\frac{\mu_m}{\mu_l} = \exp\left[\frac{K\varepsilon_s}{1-(\varepsilon_s/\varepsilon_{sc})}\right] \tag{7}$$

with two parameters correlated by

$$K = \{3.1 - 1.4\tanh[0.3(10 - 10^2 U_t)]\}/\phi \tag{8a}$$

$$\varepsilon_{sc} = \{1.3 - 0.1\tanh[0.5(10 - 10^2 U_t)]\}\varepsilon_{s0} \tag{8b}$$

where U_t is in m/s. The gas holdup in slurry bubble columns at elevated pressures can be calculated by using the empirical correlation developed in our group by Luo et al. (1999):

$$\frac{\varepsilon_g}{1-\varepsilon_g} = \frac{2.9\left(\frac{u_g^4\rho_g}{\sigma g}\right)^{\alpha}\left(\frac{\rho_g}{\rho_m}\right)^{\beta}}{[\cosh(Mo_m^{0.054})]^{4.1}} \tag{9}$$

where Mo_m is the modified Morton number for the slurry phase, $(\xi\mu_l)^4 g/\rho_m\sigma^3$, and

$$\alpha = 0.21Mo_m^{0.0079} \text{ and } \beta = 0.096Mo_m^{-0.011}. \tag{10}$$

ξ is a correction factor that accounts for the effect of particles on slurry viscosity:

$$\ln\xi = 4.6\varepsilon_s\{5.7\varepsilon_s^{0.58}\sinh[-0.71\exp(-5.8\varepsilon_s)\ln Mo^{0.22}] + 1\} \tag{11}$$

where Mo is the Morton number of the liquid, $g\mu_l^4/\rho_l\sigma^3$. This correlation is obtained based on numerous experimental data on gas holdup in high-pressure systems. The experimental data on gas holdup have been given in Luo et al. (1999), and the correlation can accurately predict gas holdup at high pressures, including the conditions of this study.

The comparison between the experimental data and the correlation calculation is given in Figure 4, which shows that the deviation in the predictions is within ±20%, and the average deviation is 6.9%. The comparison of the predictions based on the correlation proposed by Deckwer et al. (1980) (i.e., Eq. 1) and that obtained in this study (Eq. 3) is provided in Figure 5. The correlation proposed by Deckwer et al. (1980) does not account for the effect of changes in pressure on the heat transfer coefficient. The correlation obtained in this study can reasonably predict the pressure effect in such systems.

Heat Transfer Model: A consecutive film and surface renewal model originally developed by Wasan and Ahluwalia (1969) could be used to analyze heat transfer behavior in bubble columns. The schematic diagram of this model is shown in Figure 6. The model assumes that a thin liquid film with a thickness of δ surrounds the heating surface, and liquid elements are in contact with the outer surface of the film via the bubble motion or liquid turbulence. The liquid elements contact the film for a short time, t_c, and then are replaced by fresh liquid elements from the bulk fluid. During the contact, the heat is transferred to the bulk liquid through conduction in the liquid film and through unsteady state conduction in the liquid elements. Based on the energy balance, the heat transfer coefficient can be expressed in terms of the physical properties of the liquid, the film thickness, and the contact time between the liquid elements and the film (Wasan and Ahluwalia, 1969):

$$h_w = \frac{2k_l}{\sqrt{\pi\alpha t_c}} + \frac{k_l\delta}{\alpha t_c}\left[e^{\alpha t_c/\delta^2}\left(1 - erf\frac{\sqrt{\alpha t_c}}{\delta}\right) - 1\right]. \tag{12}$$

Based on Eq. (12), the heat transfer coefficient depends on the film thickness and contact time between the liquid elements and the film. Thinner film and shorter contact time lead to a higher heat transfer rate. When the physical properties of the liquid-solid suspension are used in Eq. (12), this model can also predict the heat transfer coefficient in slurry bubble columns.

Based on the border diffusion layer model (Azbel, 1981), the order of magnitude of the film thickness may be estimated by (Kumar and Fan, 1994):

$$\delta = \frac{6.14L}{\mathrm{Re}_m^{3/4}\,\mathrm{Pr}_m^{1/3}} \tag{13}$$

where Re_m is based on the length of the heat transfer probe, i.e., $\rho_m L u_b/\mu_m$, and L is the length of the heat transfer probe. The physical properties of the suspension, such as ρ_m, C_{pm}, k_m and μ_m, are calculated based on the corresponding properties of the liquid and solid phases and the solids concentration, as shown in Eqs. (4) ~ (7).

The contact time between the liquid elements and the film is assumed to be equal to the contact time between the bubbles and the film, when the bubble motion is considered the driving force of the liquid element replacement, with negligible effects of liquid turbulence. Based on this consideration, the contact time can be estimated by the following equation (Kumar and Fan, 1994):

$$t_c = \frac{L}{u_b} \tag{14}$$

where u_b is the actual bubble rise velocity in a stream of bubbles. If the effects of pressure on the liquid properties and the bubble characteristics such as bubble size and bubble rise velocity are known, this model may be used to illustrate the heat transfer behavior in a high-pressure system.

In slurry bubble columns, the bubble size is typically related to the physical properties of gas and liquid phases, gas velocity and solids concentration. Fukuma et al. (1987) measured the bubble size and bubble rise velocity in a slurry bubble column at ambient pressure with a dual-electroresistivity probe. Basing their work on the analysis of the drift flux of gas, they found that the mean bubble rise velocity can be related to the gas holdup in the column:

$$u_b \propto \frac{u_g(1-\varepsilon_g)}{\varepsilon_g}. \tag{15}$$

Considering the effect of pressure, an empirical equation accounting for the mean bubble rise velocity in slurry bubble columns is proposed to be of the following form:

$$u_b = \alpha\left[\frac{u_g\left(1-\varepsilon_g\right)}{\varepsilon_g}\right]^{\beta}. \tag{16}$$

α and β in the equation are obtained by fitting experimental data as $\alpha = 0.8$ and $\beta = 0.5$. The gas holdup in slurry bubble columns at elevated pressures can be calculated by using Eq. (9).

Based on Eqs. (12) - (14) and (16), the heat transfer coefficient under high-pressure conditions can be estimated. The heat transfer coefficients in slurry bubble columns predicted by the model are also shown in Figure 1 by solid lines. The symbols represent the experimental data. It can be seen that the prediction is in good agreement with the experimental data. The comparison between the experimental data and model predictions is provided in Figure 7. The average deviation is less than 10%. In the heat transfer model, some assumptions or simplifications need to be made in order to estimate the film thickness and the contact time, such as ignoring the liquid circulation, and assuming uniform bubble size and bubble rise velocity. The model predictions can be further improved if the internal circulation of liquid flow and the bubble size distribution can be incorporated into the model.

Based on the model, the heat transfer resistance consists of film resistance and resistance due to unsteady-state conduction through the liquid elements. The comparison of heat transfer resistance due to the film (δ/k_m) with the total heat transfer resistance ($1/h_w$) is provided in Figure 8. The figure shows that film resistance accounts for 68 - 85% of the total heat transfer resistance under various operating conditions in this study. Thus, it can be concluded that heat transfer in high-pressure slurry bubble columns is predominantly determined by conduction through the fluid film surrounding the heating surface. The film thickness and contact time between the fluid elements and the film estimated by the model under various operating conditions are provided in Figure 9. This figure shows that the film thickness and contact time are typically in the ranges of 0.1 - 0.3 mm and 0.02 - 0.1 s, respectively. The figure also shows that the bubble rise velocity estimated by the proposed equation, i.e., Eq. (16), is within 0.3 - 1.2 m/s, which agrees well with the literature data given in Fan et al. (1999). Figure 10 shows the comparison of the actual bubble rise velocity predicted by Eq. (16) and the bubble swarm velocity (i.e., u_g/ε_g) reported in the literature in high-pressure bubble columns. It can be seen that Eq. (16) can reasonably predict the magnitude of bubble rise velocity and the trend of the pressure effect on bubble rise velocity.

It is known that when pressure increases, liquid viscosity increases and bubble rise velocity decreases, as shown in Figure 10. The variations in liquid viscosity and bubble rise velocity result in a thicker film and longer contact time at higher pressures, based on Eqs. (13) and (14). Therefore, from the film and surface renewal model (Eq. 12), the heat transfer rate decreases with increasing pressure due to an increase in film thickness and in contact time between the

fluid elements and the film. It is also noted that both liquid viscosity and bubble rise velocity affect the film thickness according to the relation derived from Eq. (13):

$$\delta \propto u_b^{-3/4} \mu_m^{5/12}. \tag{17}$$

For instance, when the pressure increases from ambient pressure to 4.2 MPa, the liquid viscosity increases from 0.019 to 0.024 Pa·s, an increase of 26% at 35°C in gas-liquid systems, which would result in a 57% increase in the film thickness, based on Eq. (17). Meanwhile, bubble rise velocity decreases from 0.7 to 0.3 m/s, a decrease of 57%, as shown in Figure 10, which would result in a 66% increase in film thickness. Therefore, the variations in both liquid viscosity and bubble rise velocity are important in accounting for the change in film thickness with pressure.

Notations

C_{pl} heat capacity of liquid, J/(kg·K)
C_{pm} heat capacity of liquid-solid suspension, J/(kg·K)
C_{ps} heat capacity of solids, J/(kg·K)
d_b bubble diameter, m
Fr Froude number, $\frac{u_g^2}{g d_b}$
g gravitational acceleration, m/s^2
h_w time-averaged heat transfer coefficient, W/(m^2·K)
K proportionality constant defined in Eq. (8a), dimensionless
k_l thermal conductivity of liquid, W/(m·K)
k_m thermal conductivity of liquid-solid suspension, W/(m·K)
k_s thermal conductivity of solids, W/(m·K)
L vertical length of heating surface, m
Mo Morton number based on liquid properties, $\frac{g\mu_l^4}{\rho_l \sigma^3}$
Mo_m modified Morton number based on slurry properties, $\frac{(\xi\mu_l)^4 g}{\rho_m \sigma^3}$
P system pressure, Pa
Pr Prandtl number based on liquid properties, $\frac{C_{pl}\mu_l}{k_l}$
Pr_m Prandtl number based on slurry properties, $\frac{C_{pm}\mu_m}{k_m}$
Re Reynolds number based on liquid properties, $\frac{u_g d_b \rho_l}{\mu_l}$
Re_m Reynolds number based on slurry properties, $\frac{u_g d_b \rho_m}{\mu_m}$
St Stanton number based on liquid properties, $\frac{h_w}{\rho_l C_{pl} u_g}$

St_m Stanton number based on slurry properties, $\frac{h_w}{\rho_m C_{pm} u_g}$

T_b temperature of the bulk fluid, K
t_c contact time between the liquid elements and the film, s
T_s temperature of the heating surface, K
T system temperature, K
u_b actual bubble rise velocity in a stream of bubbles, m/s
u_g superficial gas velocity, m/s
U_t particle terminal velocity in liquid, m/s

Greek Letters

α thermal diffusivity of liquid, $\frac{k_l}{\rho_l C_{pl}}$, m^2/s

α_m thermal diffusivity of liquid-solid suspension, $\frac{k_m}{\rho_m C_{pm}}$, m^2/s

δ film thickness, m
ε_g gas holdup, dimensionless
ε_s solids concentration, dimensionless
ε_{sc} critical solids holdup, dimensionless
ε_{s0} solids holdup at incipient fluidization/packed state, dimensionless
ϕ particle sphericity, dimensionless
μ_l liquid viscosity, Pa·s
μ_m viscosity of liquid-solid suspension, Pa·s
ρ_g gas density, kg/m^3
ρ_l liquid density, kg/m^3
ρ_m density of liquid-solid suspension, kg/m^3
ρ_s solids density, kg/m^3
σ surface tension, N/m
ξ parameter accounting for the effect of particles on the viscosity, dimensionless
ω_s weight fraction of the solid phase, dimensionless

Literature Cited

Azbel, D., "Two-phase flows in chemical engineering," Cambridge University Press: Cambridge, UK (1981).

Deckwer, W. D., "On the mechanism of heat transfer in bubble column reactors," *Chem. Eng. Sci.* 35, 1341 (1980).

Deckwer, W. D., Y. Louisi, A. Zaidi, and M. Ralek, "Hydrodynamic properties of the Fischer-Tropsch slurry process," *Ind. Eng. Chem. Proc. Des. Dev.* 19, 699 (1980).

Fan, L. S., G. Q. Yang, D. J. Lee, K. Tsuchiya, and K. Luo, "Some aspects of high-pressure phenomena of bubbles in liquids and liquid-solid suspensions," *Chem. Eng. Sci.* 54, 4681 (1999).

Fukuma, M., K. Muroyama, and A, Yasunishi, "Properties of bubble swarm in a slurry bubble column," *J. Chem. Eng. Japan* 20, 28 (1987).

Hart, W. F., "Heat transfer in bubble-agitated systems: a general correlation," *Ind. Eng. Chem. Process Des. Dev.* 15, 109 (1976).

Kang, Y., I. S. Suh, and S. D. Kim, "Heat transfer characteristics of three-phase fluidized beds," *Chem. Eng. Comm.* 34, 1 (1985).

Kast, W., Analyse des warmeubergangs in blasensaulen," *Int. J. Heat Mass Transfer* 5, 329 (1962).

Kato, Y.; K. Uchida, and S. Morooka, "Liquid holdup and heat transfer coefficient between bed and wall in liquid-solid and gas-liquid-solid fluidized beds," *Powder Technology* 28, 173 (1981).

Kumar, S., and L.S. Fan, "Heat transfer characteristics in viscous gas-liquid and gas-liquid-solid systems," *AIChE J.* 40, 745 (1994).

Kumar, S., K. Kusakabe, K. Raghunathan, and L.S. Fan, "Mechanism of heat transfer in bubbly liquid and liquid-solid systems: single bubble injection," *AIChE J.* 38, 733 (1992).

Letzel, H. M., J. C. Schouten, C. M. van den Bleek, R. Krishna, "Influence of elevated pressure on the stability of bubbly flows," *Chem. Eng. Sci.* 52, 3733 (1997).

Luo, X.; D. J. Lee, R. Lau, G. Q. Yang, and L. S. Fan, "Maximum stable bubble size and gas holdup in high-pressure slurry bubble columns," *AIChE J.* 45, 665 (1999).

Luo, X., J. Zhang, K. Tsuchiya, and L. S. Fan, "On the rise velocity of bubbles in liquid-solid suspensions at elevated pressure and temperature," *Chem. Eng. Sci*. 52, 3693 (1997).

Magiliotou, M., Y. M. Chen, and L. S. Fan, "Bed-immersed object heat transfer in a three-phase fluidized bed," *AIChE J.* 34, 1043 (1988).

Reid, R. C., J. M. Prausnitz, and T. K. Sherwood, *The Properties of Gases and Liquids,* McGraw-Hill: New York (1977).

Saxena, S. C., N. S. Rao, and A. C. Saxena, "Heat transfer from a cylindrical probe immersed in a three-phase slurry bubble column," *Chem. Eng. J.* 44, 141 (1990).

Shaykhutdinov, A. G., N. U. Bakirov, and A, G. Usmanov, "Determination and mathematical correction of heat transfer coefficients under conditions of bubble flow, cellular, and turbulent foam," *Int. Chem. Eng.* 11, 641 (1971).

Steiff, A., and P. M. Weinspach, "Heat transfer in stirred and non-stirred gas-liquid reactors," *Ger. Chem. Eng.* 1, 150 (1978).

Tareef, B. M., "Thermal conductivity of colloidal systems," *Colloidal J. of USSR* 6, 545 (1940).

Wasan, D. T. and M. S. Ahluwalia, "Consecutive film and surface renewal mechanism for heat and mass transfer from a wall," *Chem. Eng. Sci.* 24, 1535 (1969).

Wilkinson, P. M., and L. L. Dierendonck, L. L. "Pressure and gas density effects on bubble break-up and gas hold-up in bubble columns," *Chem. Eng. Sci.* 45, 2309 (1990).

Zehner, P., "Momentum, mass and heat transfer in bubble columns. Part 2. Axial blending and heat transfer," *Int. Chem. Eng.* 26, 29 (1986).

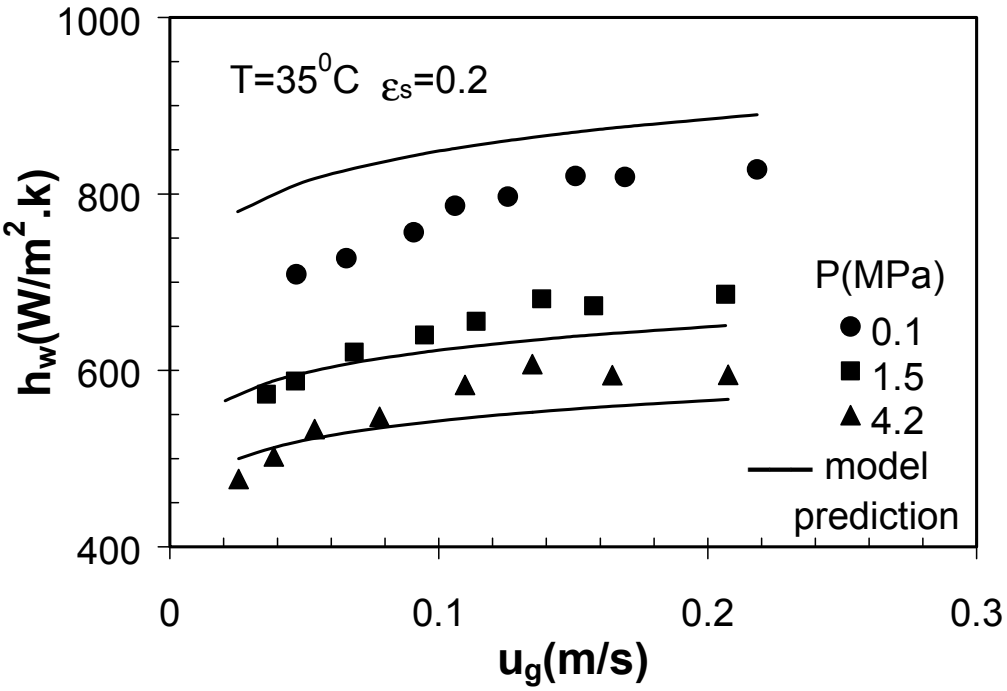

(a)

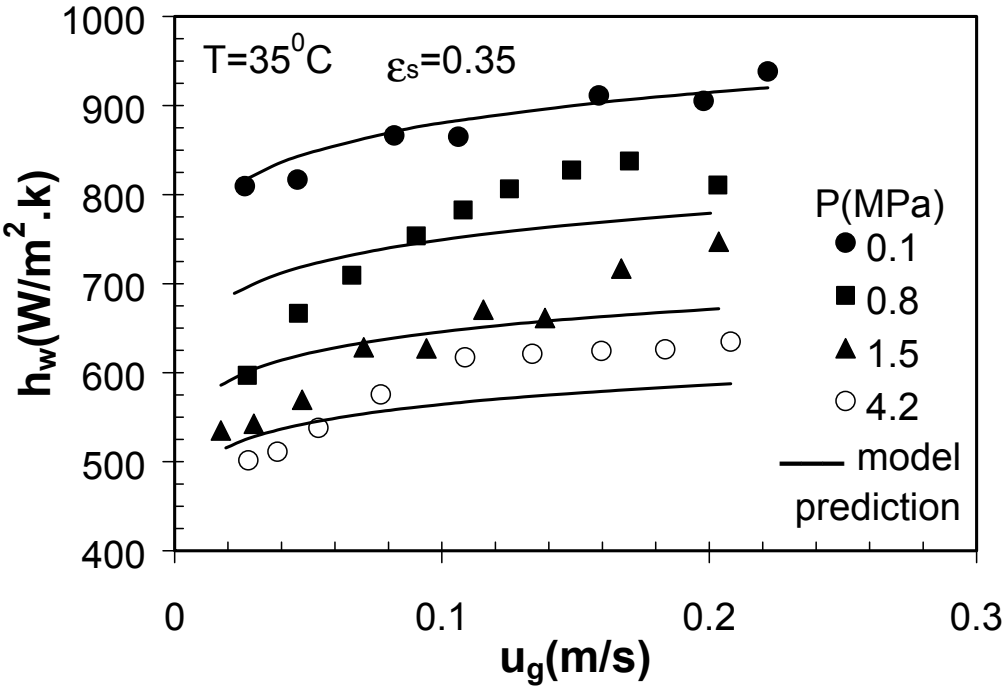

(b)

Figure 1 Pressure Effect on Heat Transfer Coefficients in Slurry Bubble Columns (T=35^{o}C): (a) ε_s=0.2; and (b) ε_s=0.35

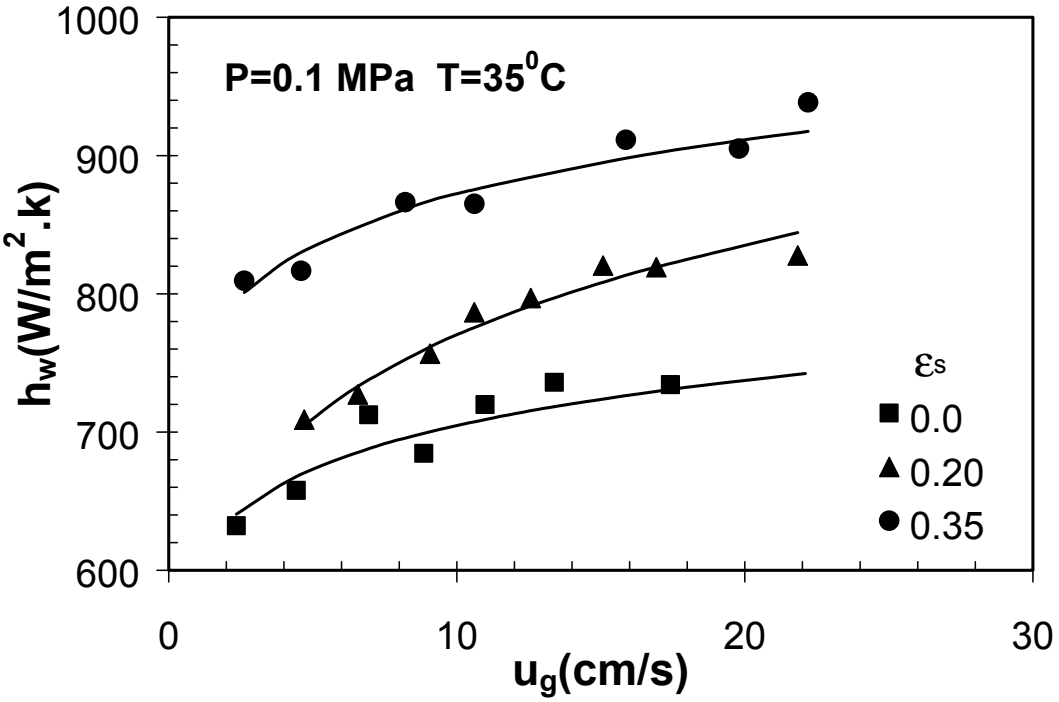

(a) ambient pressure

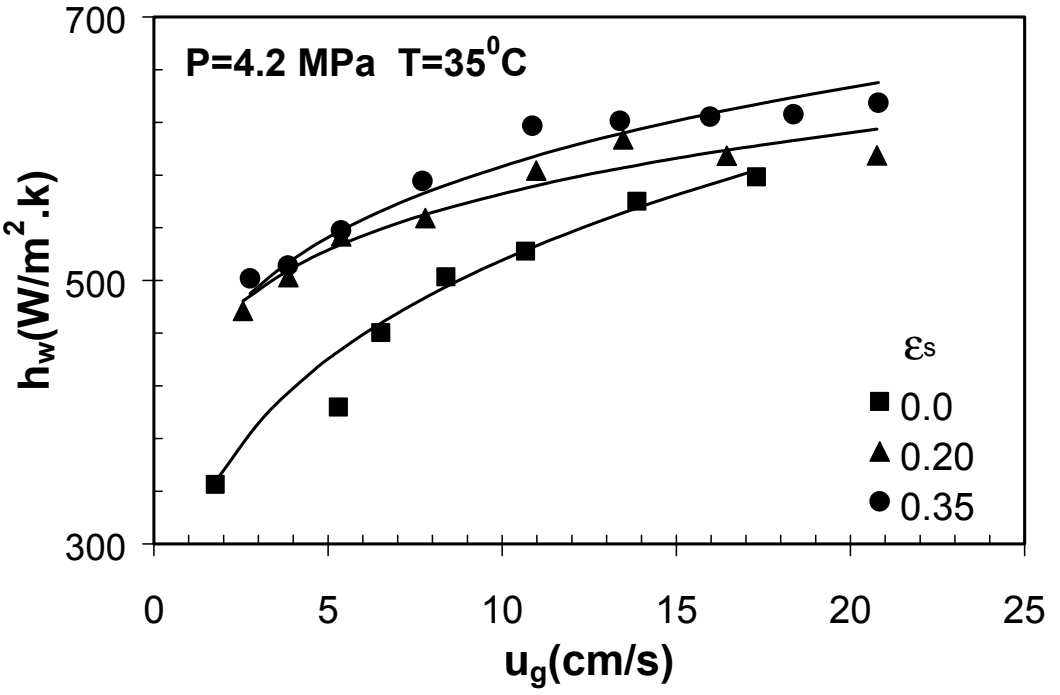

(b) high pressure

Figure 2 Heat Transfer Coefficient as a Function of Gas Velocity at Different Solids Concentrations (T=35^{o}C) under: (a) Ambient Pressure and (b) High Pressure (P=4.2 MPa)

(Solid lines are trendlines.)

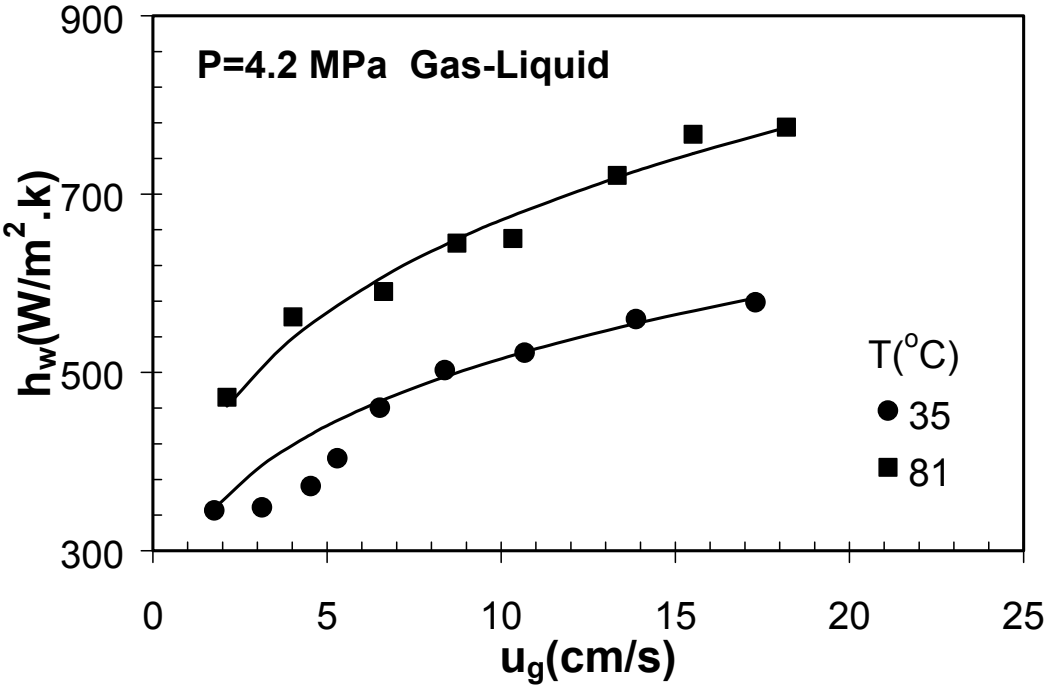

bubble columns

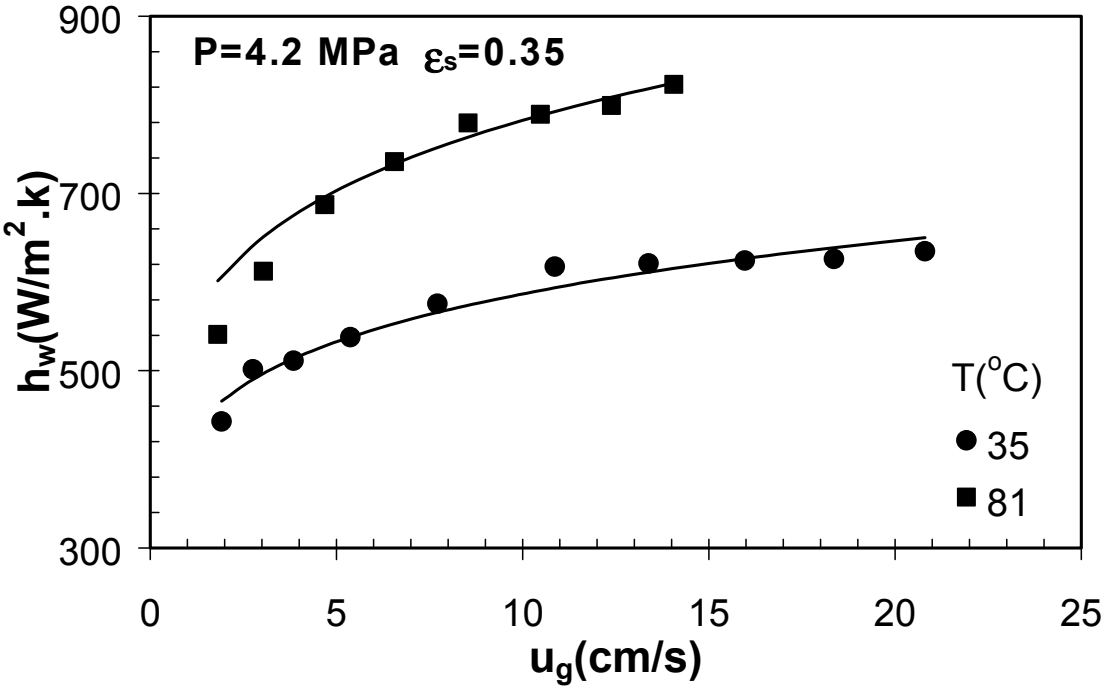

(a) slurry bubble columns

Figure 3 Heat Transfer Coefficient as a Function of Gas Velocity at Different Temperatures (P=4.2 MPa) in: (a) Bubble Columns and (b) Slurry Bubble Columns

(ε_s=0.35)
(Solid lines are trendlines.)

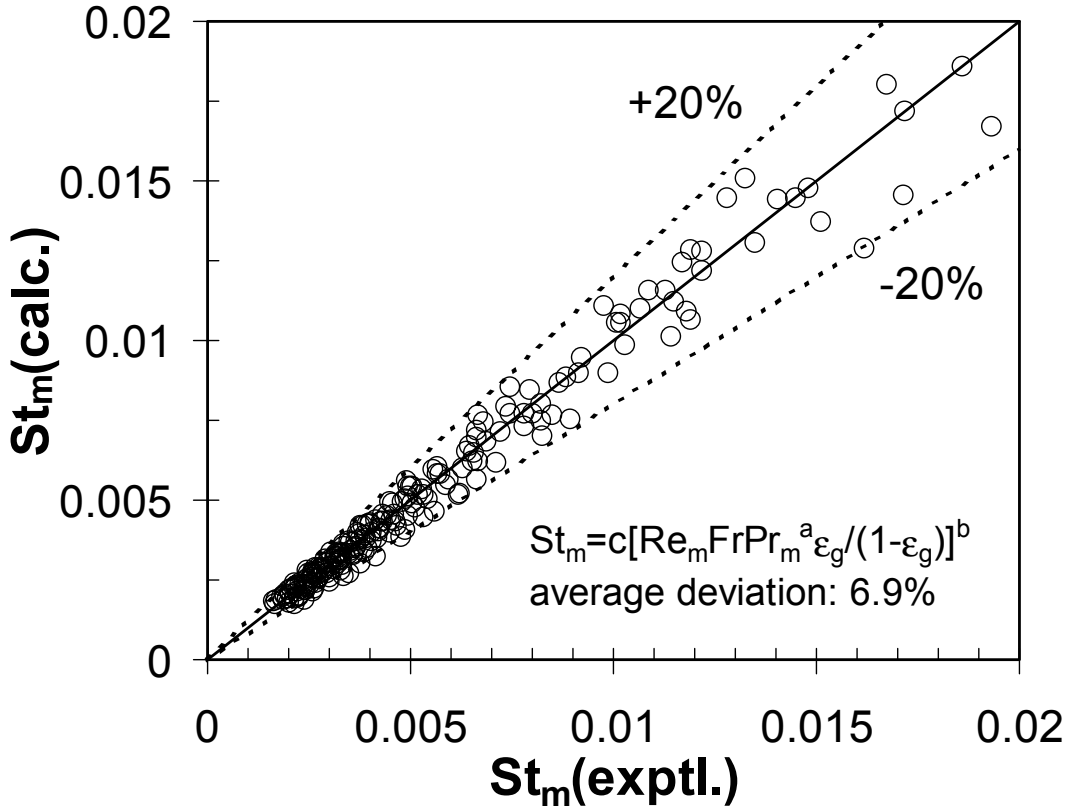

Figure 4 Comparison Between the Correlation Predictions and the Experimental Data of the Heat Transfer Coefficient in Terms of Stanton Number

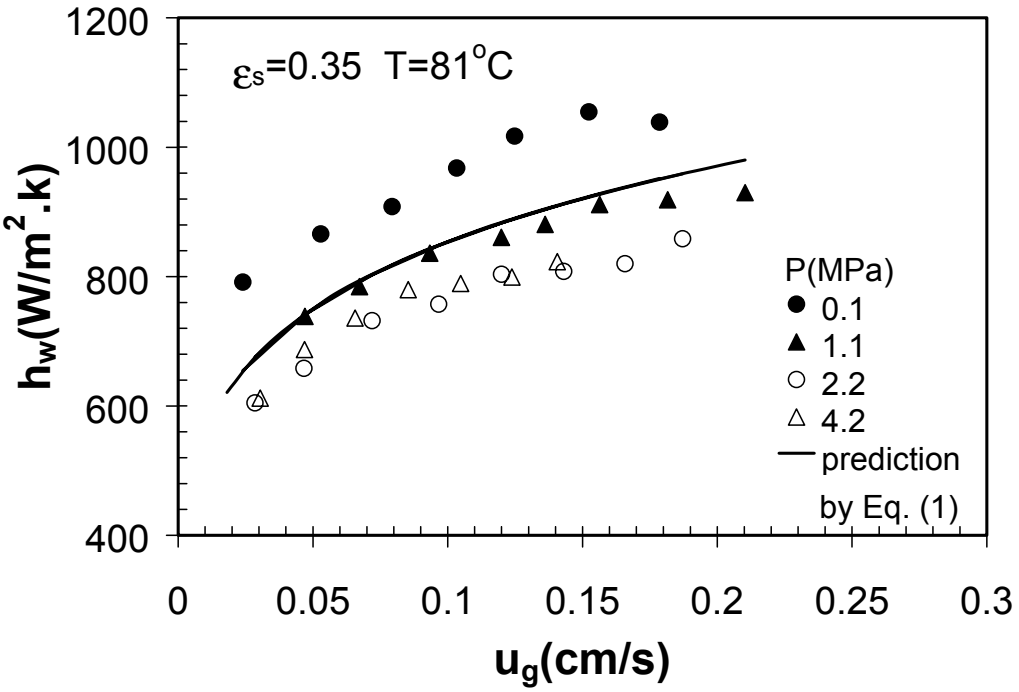

(a) Deckwer's correlation

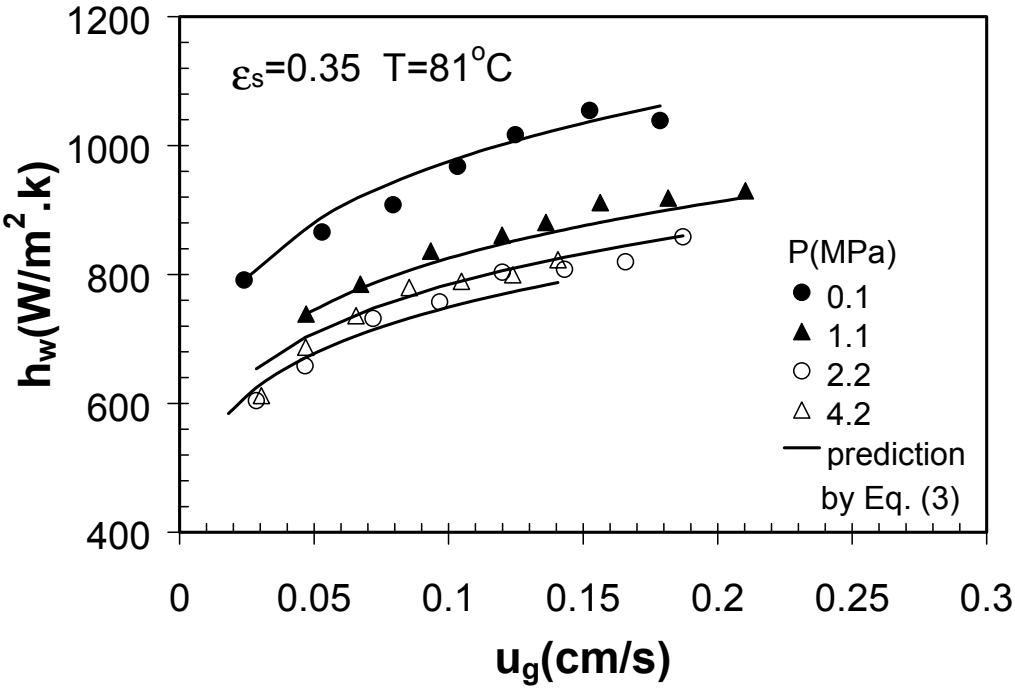

(b) Correlation proposed in this study

Figure 5 Comparison of the Predicted Results of Heat Transfer Coefficients in Slurry Bubble Columns under High Pressure and High Temperature Conditions by using (a) Deckwer's Correlation and (b) the Correlation Proposed in this Study

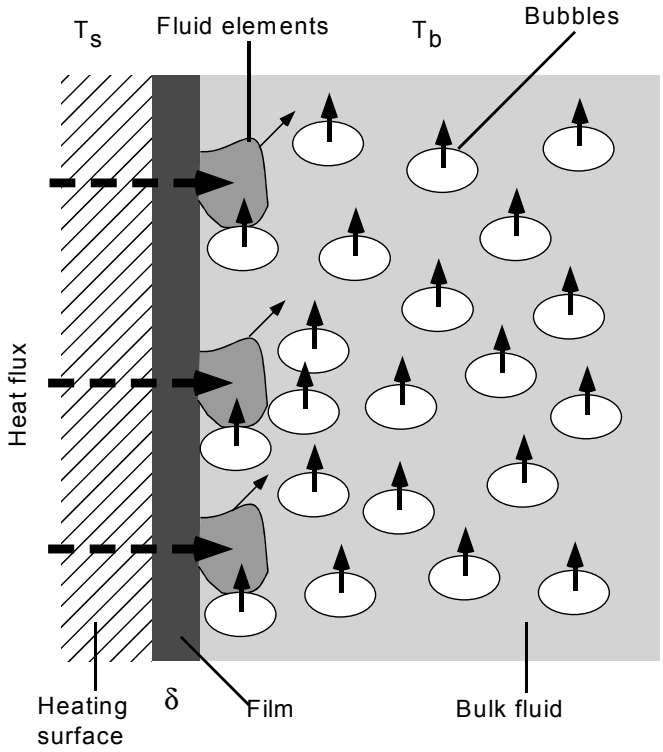

Figure 6 Schematic of the Consecutive Film and Surface Renewal Model (Wasan and Ahluwalia, 1969)

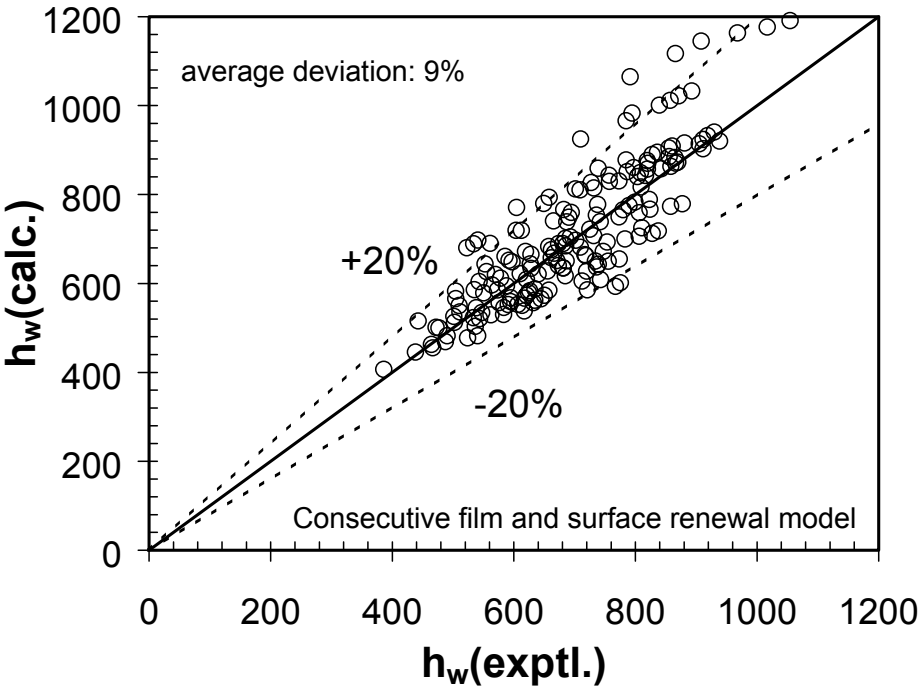

Figure 7 Comparison Between the Predictions and the Experimental Data of the Heat Transfer Coefficient based on the Consecutive Film and Surface Renewal Model

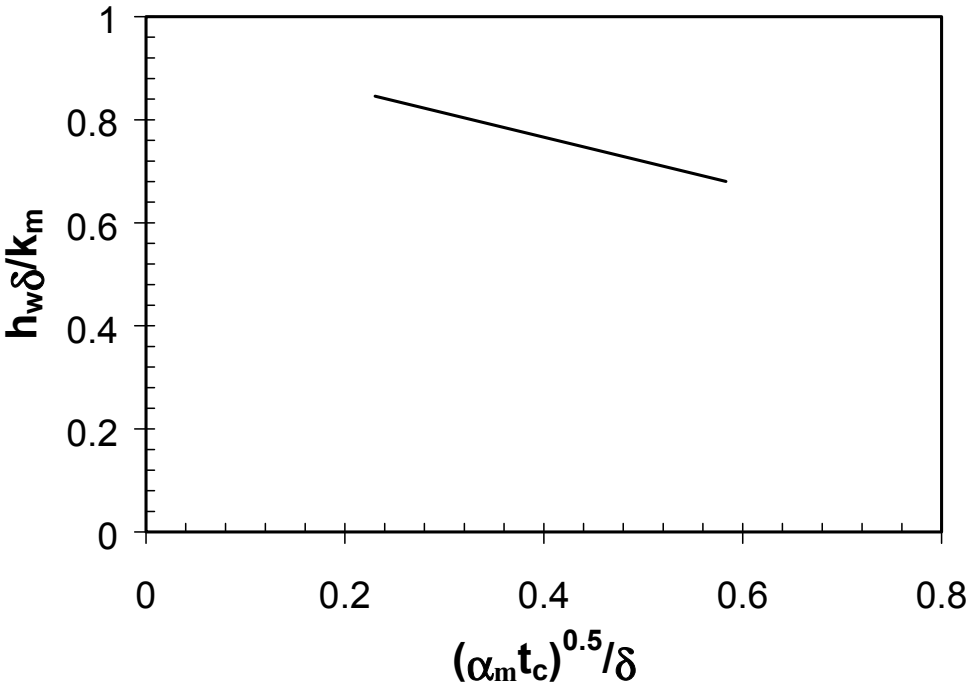

Figure 8 Comparison of Heat Transfer Resistance due to the Film with the Total Heat Transfer Resistance

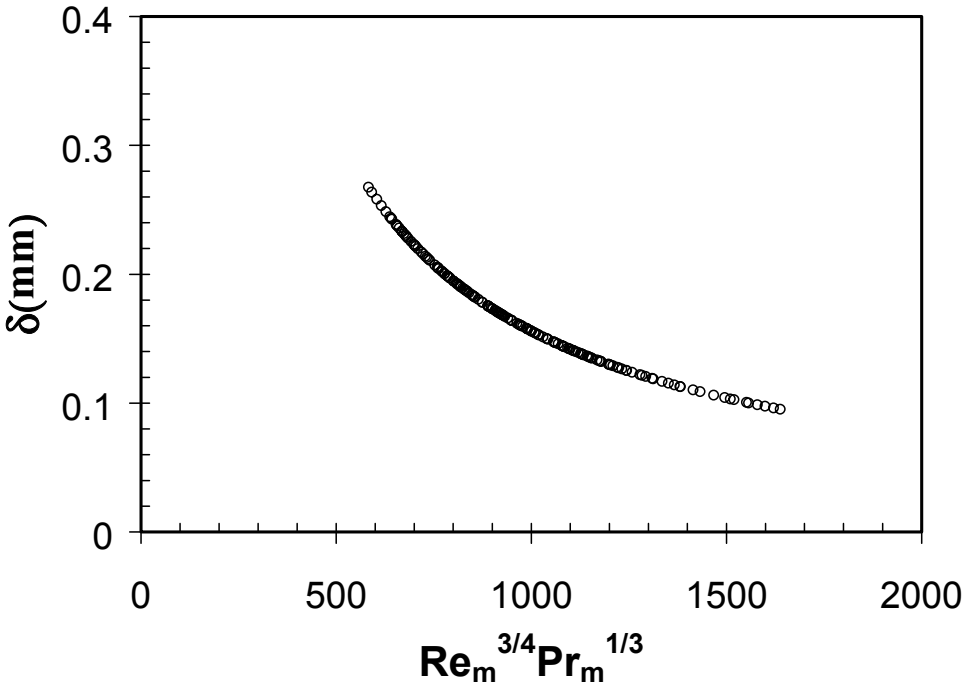

(a) film thickness

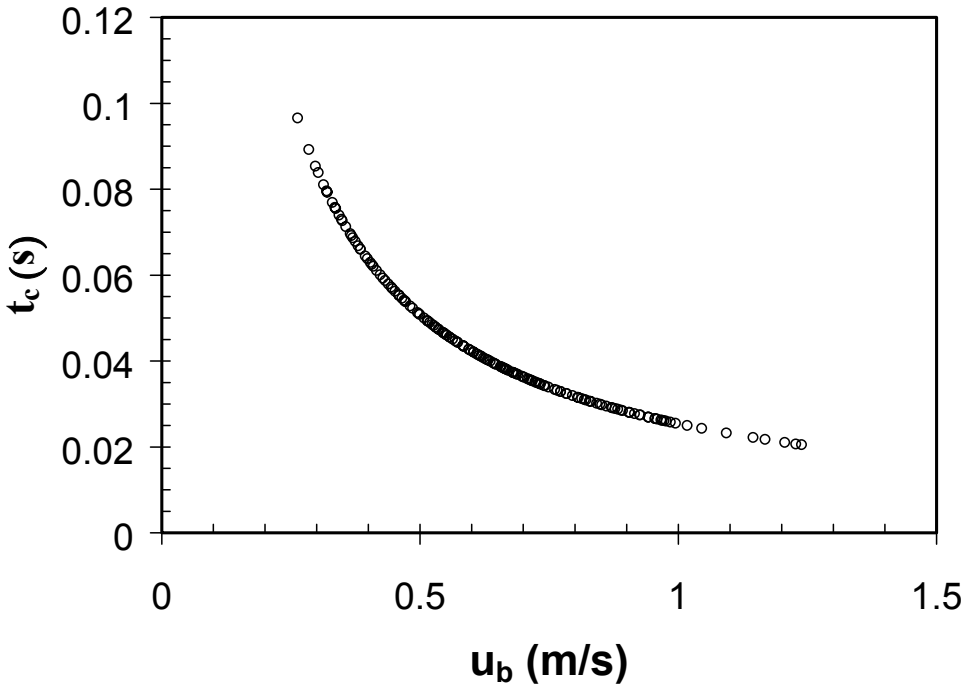

(b) contact time

Figure 9 The Typical Values of (a) Film Thickness and (b) Contact Time Between the Liquid Elements and the Film Estimated by the Model under Various Operating Conditions

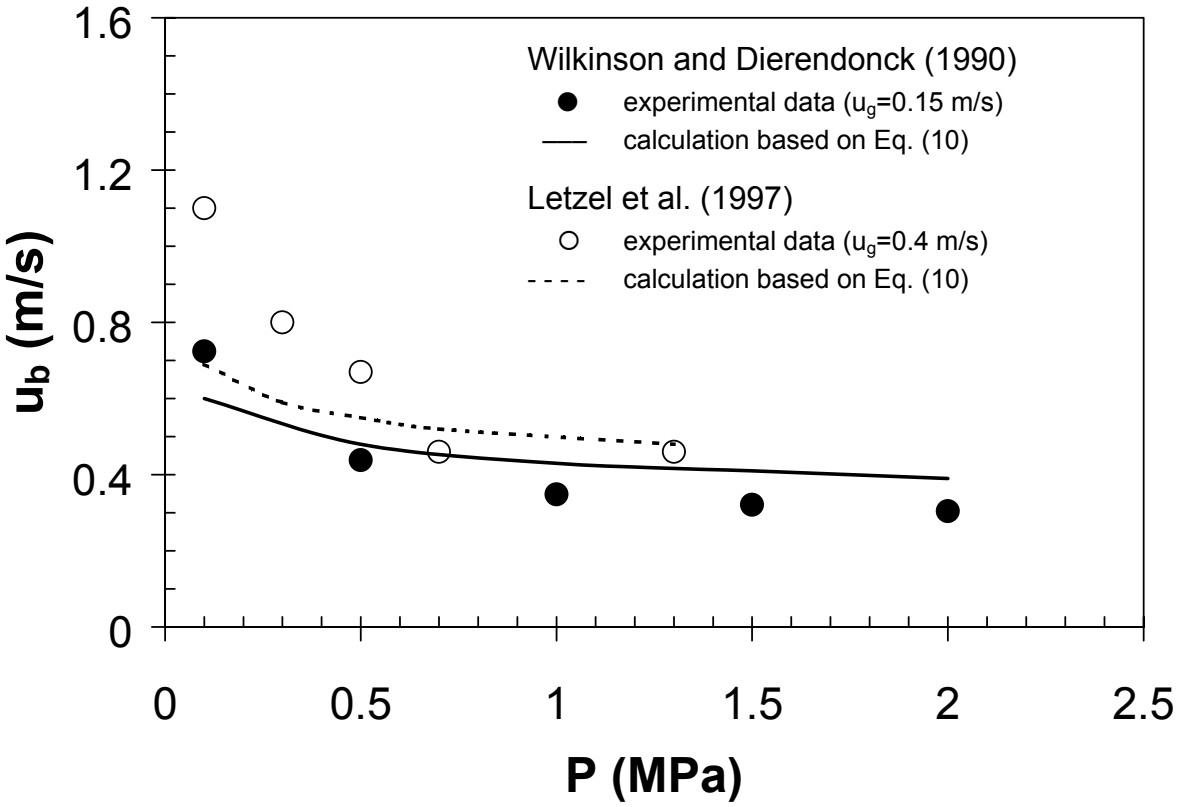

Figure 10 Comparison of the Actual Bubble Rise Velocity Predicted by Eq. (10) and the Bubble Swarm Velocity Reported in the Literature for High-Pressure Bubble Columns

Washington University in St. Louis

The report from Washington University for the period follows.

ENGINEERING DEVELOPMENT OF SLURRY BUBBLE COLUMN REACTOR (SBCR) TECHNOLOGY

Twenty First Quarterly Report
for
April 1 – June 30, 2000

(Budget Year 5: October 1, 1999 – September 30, 2000)

Chemical Reaction Engineering Laboratory
Chemical Engineering Department
Washington University

Objectives for the Fifth Budget Year

The objectives set for the Fifth Budget Year (October1, 1999 to September 30, 2000) are listed below.

- Extension of the CARPT (Computer-Aided Radioactive Particle Tracking) database to high superficial gas velocity in bubble columns
- Extension of CARPT/CT (Computed Tomography) database to gas-liquid-solid systems at high superficial gas velocity
- Evaluation of the effect of sparger design on the fluid dynamics of bubble columns using the CARPT technique
- Interpretation of LaPorte tracer data
- Further improvement in Computational Fluid Dynamics (CFD) using CFDLIB and Fluent

In this report, the research progress and achievements accomplished in the twenty-first quarter (April 1 – June 30, 2000) are summarized.

HIGHLIGHTS FOR THE 21ST QUARTER

1. Catalyst/liquid-like tracer studies during FT-IV runs

- The modified liquid/slurry mixing model as reported in the last quarterly report has been applied to simulate the catalyst and Mn_2O_3 tracer responses from Fischer-Tropsch (FT) Run 16.7. The model equations were solved by an implicit finite-difference scheme, with the liquid mixing parameters estimated from a two-fluid sub-model (Gupta et al., 2000). Comparison of model predictions with data indicates that the model is able to predict the state of the liquid mixing well.
- The higher superficial gas velocity for Run 16.7 resulted in relatively faster radial mixing compared to Run 16.6. Therefore, for Run 16.7, the agreement between simulation results and experimental data for the sidewall-middle tracer injection are considerably better than for Run 16.6. Nevertheless, bottom-middle injection is recommended for characterization of mixing of the slurry phase, and sidewall injection should be avoided.
- The fine Mn_2O_3 tracer seems to follow the liquid more closely than the catalyst particles, and in general there is better agreement between simulation results for the slurry (liquid) and experimental data for Mn_2O_3 tracer responses. However, at conditions of Run 16.7, the catalyst tracer also seems to follow the liquid closely.
- As with Run 16.6, the simulated detector responses for the upper portion of the column appear to be more diffused than the experimental data, indicating the possibility of foaming and the effect of a reduced superficial gas velocity due to some gas bypassing the top portion of the column along with the slurry.

2. Radioactive gas tracer studies during FT-IV runs

- A gas-liquid recirculation model based on a constant bubble size, describing the gas-liquid mass transfer superimposed on the turbulent mixing of the gas and liquid phases, was developed and used to simulate the gas tracer responses acquired during the FT-IV operation of the AFDU (Alternative Fuels Development Unit). The model is able to predict the characteristic features of the observed experimental responses.
- For the given gas holdup profiles and operating conditions, the sub-model for gas-liquid recirculation predicted a mean bubble size of 1.6 mm for Run 16.6 and 9.4 mm for Run 16.7.
- For Run 16.6, the predicted tracer responses based on Henry's constant of H = 0.15 are in reasonable agreement with experimental data. However, the predicted response for the thermodynamically estimated Henry's constant of H = 0.248 seems to be delayed in time. On the other hand, the predicted tracer responses for Run 16.7 based on thermodynamically predicted Henry's constant are in reasonably good agreement with experimental data, since

a higher superficial gas velocity in Run 16.7 results in satisfying the model assumptions better compared to Run 16.6.

- The lack of exact match of experimental data by the model predictions should be viewed in conjunction with the physics omitted in the simulations. Such omissions include the tracer spread due to insufficient shielding of the scintillation detectors, as well as the alternate paths available for tracer dispersion (degasser, slurry/vapor recycle) not considered in the simulations.

1. CATALYST/LIQUID-LIKE TRACER STUDIES DURING FT-IV RUNS AT AFDU IN LA PORTE, TX – CONTINUED

In the last quarterly report, we presented the analysis of the catalyst tracer responses for Run 16.6 using a mechanistic liquid/slurry mixing model. This model was modified to account for recycle by adding a section that contains the slurry recycle from the middle portion of the column to the bottom of the column. This modified model has been further employed to simulate the tracer responses for Run 16.7 for both the liquid-like (fine Mn_2O_3 powder in heat transfer oil) and catalyst tracers. These results are compared with model simulations with experimentally obtained responses.

1.1 Comparison of Experimental Tracer Responses with Simulation Results

The reactor layout and the column compartmentalization for the liquid mixing model are shown in Figures 1 and 2, respectively. These are the same as presented in the last quarterly report, but are being repeated here for easy reference. Simulations were carried out using the liquid mixing model for the operating conditions of Run 16.7 listed in Table 1. As mentioned in the previous reports, the sub-model for parameter estimation procedure requires as input the radial gas holdup profile, which is represented as

$$\varepsilon_G(\xi) = \bar{\varepsilon}_G\left(\frac{m+2}{m+2-2c}\right)\left(1-c\xi^m\right) \tag{1}$$

In Equation (1), $\bar{\varepsilon}_G$ is the volume-averaged mean gas holdup, estimated using the Differential Pressure (DP) measurements; m is the exponent which is taken as 2, as suggested by Degaleesan (1997); and c is the parameter that allows for a non-zero holdup at the wall. This is estimated using the chordal average holdup obtained with Nuclear Density Gauge (NDG) measurements. These parameters are also reported in Table 1. This table reveals a peculiar situation of higher measured average gas holdup $\left(\bar{\varepsilon}_g\big|_{DP}\right)$ in Run 16.6, executed at lower superficial gas velocity, than in the Run 16.7, which was conducted at higher U_g. Since the pressure and temperature were essentially the same in the two runs, the higher gas holdup may imply that these conditions are close to transition between bubbly and churn-turbulent flow. In the transition zone, which is known to occur at gas superficial velocities of 3-6 cm/s in water and at atmospheric pressure and at much higher gas superficial velocities at elevated pressures, different overall gas holdups are frequently observed, and poor reproducibility or

multiple holdup values are reported. These observations also mean that meaningful interpretation of the effect of gas superficial velocity on liquid or gas mixing based on Runs 16.6 and 16.7 is difficult, if not impossible, since the two runs likely did not experience the same flow regime.

Figures 3 and 4 compare the simulation results with experimental data for sidewall-middle and center-bottom injections, respectively, for the catalyst tracer. This comparison reveals that the dominant time constant is captured rather well by the model at all axial detector locations. The agreement between model predictions and data is somewhat better for the center-bottom injection (Figure 4) than for sidewall-middle injection (Figure 3), since for the former the assumptions of the model are better satisfied (more liquid radial and azimuthal mixing at the location of tracer injection). It should be recalled that our model treats the slurry as a pseudo-homogeneous mixture, so that the response of the catalyst tracer is modeled as the liquid (slurry) response. Figures 5 and 6 compare the model predictions for the slurry response (same as in Figures 3 and 4) and the experimental data for the fine Mn_2O_3 tracer that should be fully capable of following the liquid. In general the agreement between data and predictions is even better. Figures 3 and 5 also show that the model predictions for the sidewall-middle injection for the catalyst, as well as for the Mn_2O_3 tracer, are in reasonable agreement with the experimental responses, especially for levels of 54.5, 83, 116, 133, and 160.5 inches with reference to zero on the outside tape. This observation was not the case for the tracer responses obtained for sidewall injections under conditions of Run 16.6. The higher superficial gas velocity employed during Run 16.7 seems to have resulted in better radial mixing of the tracer, even for the sidewall-middle injection, thus better satisfying the model assumptions. Even though the agreement is better than that for Run 16.6, the proximity of the tracer injection point to the slurry outlet still cannot be completely captured by the employed model, and as before, we do not recommend this tracer injection point for any future studies with a net slurry recycle from the middle portion of the column.

Comparison of the tracer responses from simulations and experiments for the center-bottom injection (both for the catalyst, as well as the Mn_2O_3 tracer) reveals better agreement between data and model predictions than do the results for the sidewall-middle injection. This is not surprising since the tracer not only has sufficiently longer time to disperse radially before encountering the slurry exit, it also is mixed faster due to a higher superficial gas velocity. Comparing the tracer responses with simulation results for the catalyst and fine Mn_2O_3 particles reveals that the Mn_2O_3 particles seem to trace the liquid better, and consequently, there is better agreement of Mn_2O_3 responses with simulation results compared to catalyst responses.

For Run 16.6, comparison of the simulated responses and experimental data for levels of 191 and 215 inches, as referenced on the outside tape, indicates that the simulated tracer responses arrive earlier than do the experimental responses. These discrepancies between the simulated and measured responses for the top portion of the reactor could result from existence of a foamy structure near the gas-liquid interface. The discrepancies could also result from the fact that the effective superficial gas velocity through the upper portion of the column is lower due to some gas bypassing the reactor via the slurry outlet line.

1.2 Conclusions

The liquid/slurry mixing model was successfully employed to model the operating conditions of Run 16.7, and the results of the tracer simulations compare well with experimental data. The reasonably good agreement of the simulation results with the experimental data indicates that the mechanistic modeling of the flows used in our models offers a possibility for predicting the extent of mixing in these reactor types and a relatively simple tool for assessing reactor performance.

The fine Mn_2O_3 particles follow the liquid phase very well; consequently the tracer responses, obtained by employing these particles as tracers, are much better predicted by the mixing model, which is based on the assumption of a pseudo-homogeneous slurry phase.

Comparison of the simulation results with experimental data indicates that model assumptions are violated for tracer injections very close to the slurry exit (as for the sidewall tracer injection), and this observation manifests itself in poor agreement between simulated and experimental data. However, the model assumptions seem to hold well for the tracer injection into the reactor bottom, and very good agreement is obtained between simulated and experimental data. We recommend that for future tracer tests on this unit with a finite slurry outflow, sidewall tracer injections into the middle portion of the reactor not be pursued unless comparison with 3-D (three-dimensional) mixing models is being considered. These results indicate that a reliable estimate of the state of liquid mixing can be obtained by using the fine Mn_2O_3 particles. Whether catalyst particles follow the liquid can be assessed effectively via catalyst tracer studies. At the conditions of Run 16.7, the catalyst seems to follow the liquid well.

2. RADIOACTIVE GAS TRACER STUDIES DURING FT-IV RUNS AT THE AFDU IN LAPORTE, TEXAS

In this section, the analysis of the gas tracer responses from Runs 16.6 and 16.7 is presented using a mechanistic gas-liquid/slurry mixing model with interphase mass transfer to account for the finite solubility of the gas tracer (Ar^{41}). The compartmentalization of the reactor volume is shown in Figure 7, and the model equations for each compartment are summarized in Table 2. Detailed derivation of the gas-liquid recirculation model equations, the solution procedure and parameter estimation are described elsewhere (Gupta et al., 2000).

2.1 Comparison of Experimental Tracer Responses with Simulation Results

Run 16.6

Figures 8a to 8h compare the simulation results with experimental data for the radioactive gas tracer injected below the gas sparger. Figure 8 shows that the model predictions are in good agreement with the experimental responses for zero and small values of the Henry's constant at lower reactor levels, while for higher levels, a Henry's constant of 0.15 (dimensionless) seems to bring the predictions closer to data. However, for the

thermodynamically estimated Henry's constant (H = H* = 0.248), the predicted responses are delayed in time when compared to the experimental data. The reason for this discrepancy could lie in the errors associated with the estimation of the Henry's constant, in addition to the excessive spreading of the recorded experimental radiation intensity responses due to insufficient shielding of the scintillation crystals.

Run 16.7

Figures 9a to 9h compare the simulation results with experimental data for the radioactive gas tracer injected below the gas sparger. Figure 9 indicates that at the lowest tracer-monitoring level, the model simulations are in good agreement with the experimental responses for smaller values of the Henry's constant than predicted by thermodynamic calculations; in addition, for the middle monitoring levels, a Henry's constant of 0.15 (dimensionless) provides the best match between data and simulations. The thermodynamically estimated Henry's constant (H*=0.245) results in reasonable predictions of the data at the middle levels and in excellent agreement with the experimental data at the two highest levels in the column. The mismatch between simulated and experimental tracer curves is well within the thermodynamic estimation accuracy of the Henry's constant. Moreover, additional spreading of the experimentally determined radiation intensity responses is caused by insufficient shielding of the scintillation detector crystals.

2.2 Conclusions

The predicted tracer responses for the thermodynamically estimated Henry's constant are slightly delayed in time compared to the experimental responses. A Henry's constant of about 0.2 appears to provide the best match of predicted responses with the simulated ones for most monitoring levels. The reasonably good agreement of the simulation results with the experimental data indicates that the mechanistic modeling of gas-liquid flows in slurry bubble columns provides a relatively simple tool for assessing the extent of mixing to about within 20% in these reactor types.

Plans for the Next Quarter

In the next quarter, experiments are planned to study pressure and distributor effects on gas holdup in bubble columns via computed tomography.

Nomenclature

a	specific interfacial area, cm^{-1}
C	concentration, moles/cm^3
c	parameter in the holdup profile to allow non-zero holdup at the wall
d_B	bubble diameter, cm
D_C	column diameter, cm
$\overline{D}_{rr}$	radial turbulent diffusivity, cm^2/s
$\overline{D}_{xx}$	axial turbulent eddy diffusivity of liquid, cm^2/s
k_l	mass transfer coefficient, cm/s
L	dispersion height between the two CSTs, cm

l	mixing length, cm
m	power law exponent in the radial gas holdup profile
Q	flow rate, cm^3/s
R	column radius, cm
r	radial position in the column, cm
r'	radius where the liquid velocity profile inverts, cm
r''	radius where the gas velocity profile inverts, cm
t	time, sec
$U_{G,sup}$	gas superficial velocity, cm/s
$U_{L.sup}$	liquid superficial velocity, cm/s
u	axial velocity, cm/s
$\bar{u}$	radially averaged mean axial velocity, cm/s
V_a	volume of the CST representing the distributor zone, cm^3
V_b	volume of the CST representing the disengagement zone, cm^3
x	axial position in the column, cm

Greek Symbols

ε	local phase holdup
$\bar{\varepsilon}$	radially averaged phase holdup
ϕ	fraction of the column diameter
ρ	density, g/cm^3
τ	shear stress, $g/(cm.s^2)$
ξ	dimensionless radius

Subscripts

CST	well-mixed distributor and disengagement zones, a and b
in	reactor inlet
G, g	gas
ga	gas phase in the distributor zone, CST a
gb	gas phase in the disengagement zone, CST b
g1	up-flowing gas
g2	down-flowing gas
L, l	liquid
la	liquid phase in the distributor zone, CST a
lb	liquid phase in the disengagement zone, CST b
l1	up-flowing liquid
l2	down-flowing liquid

Acronyms

AFDU – Alternative Fuels Development Unit
CARPT – Computer-Aided Radioactive Particle Tracking
CFD – Computational Fluid Dynamics
CFDLIB – CFD codes
CST – well-mixed distributor and disengagement zones

CT – Computed Tomography
DP – Differential Pressure
FT – Fischer-Tropsch
H – Henry's Constant
NDG – Nuclear Density Gauge
3-D – three-dimensional
Mn_2O_3 – manganese trioxide

References

Degaleesan, S., "Fluid dynamic measurements and modeling of liquid mixing in bubble columns," *D.Sc. Thesis*, Washington University (1997).

Gupta, P., B. Ong, M.H. Al-Dahhan, M.P. Dudukovic, and B.A. Toseland, "Hydrodynamics of churn-turbulent bubble columns: gas-liquid recirculation and mechanistic modeling," accepted for publication in a topical issue of *Catalysis Today* (2000).

Table 1 Reactor Operating Conditions during Tracer Tests

	Run 16.6	Run 16.7
Operating Temperature (^{o}K)	532.0	534.2
Operating Pressure (MPa)	4.996	4.997
Inlet Superficial Gas Velocity (cm/s)	12.81	18.23
Outlet Superficial Gas Velocity (cm/s)	9.89	15.21
Average Superficial Gas Velocity (cm/s)	11.35	16.72
Liquid/Slurry Superficial Velocity (cm/s)	0.727	0.722
Height of Dispersed Media (cm)	631	633
$\bar{\varepsilon}_G\big\vert_{NDG}$	0.529	0.507
$\bar{\varepsilon}_G\big\vert_{DP}$	0.494	0.464
m	2	2
c, estimated from $\bar{\varepsilon}_G\big\vert_{Chord}$	0.351	0.435

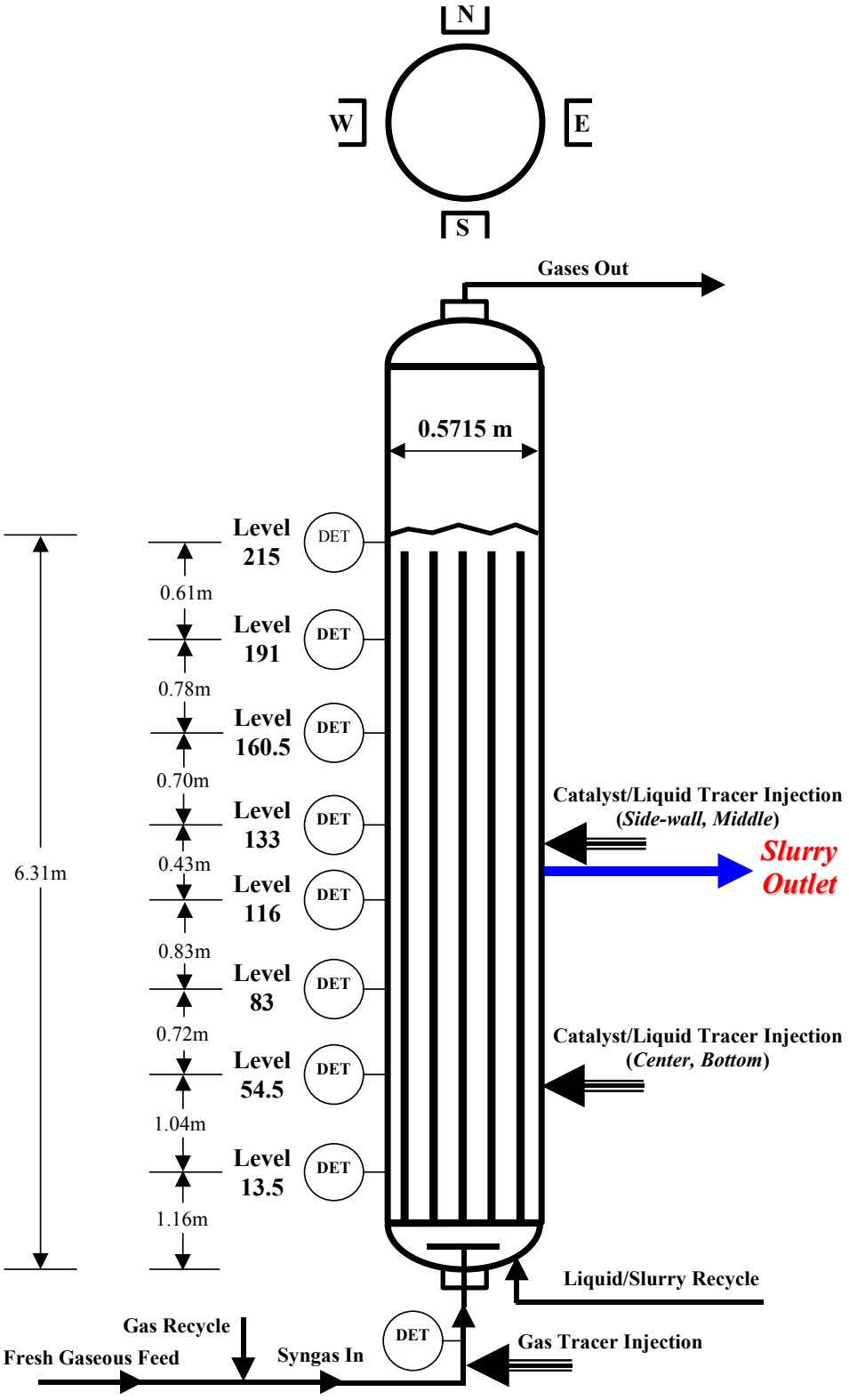

Figure 1 Schematic of the Reactor along with the Placement of the Scintillation-Detectors for Measuring Tracer Responses

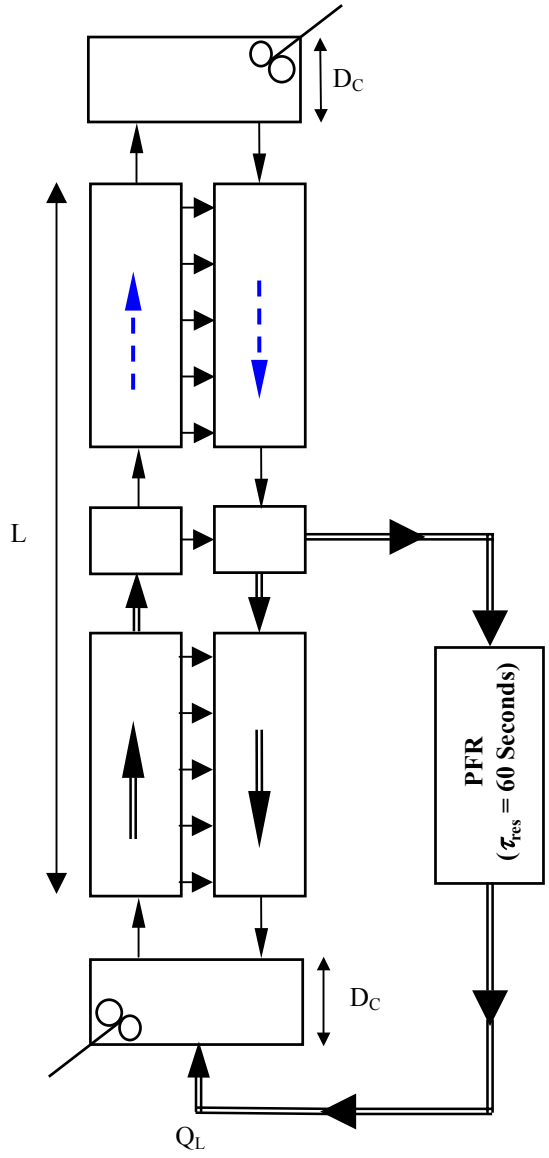

Figure 2 Schematic of the Reactor Compartmentalization for the Modified Liquid/Slurry Mixing Model

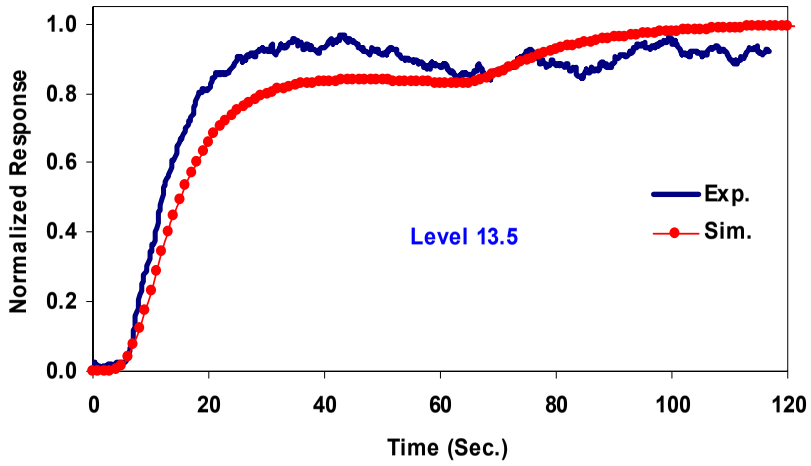

(a)

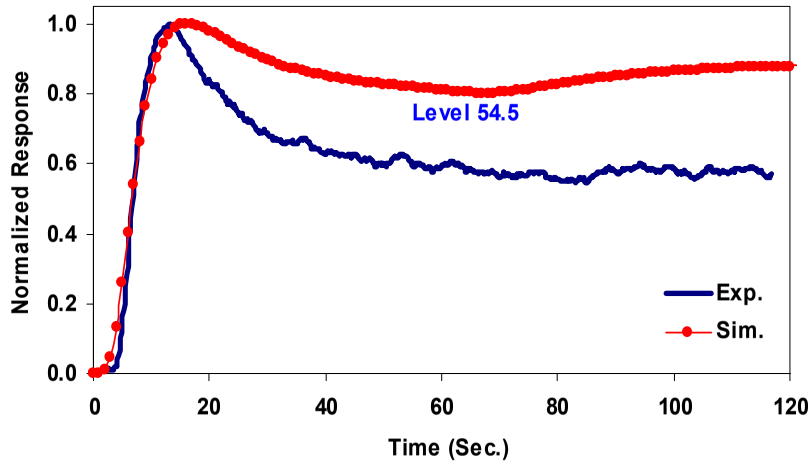

(b)

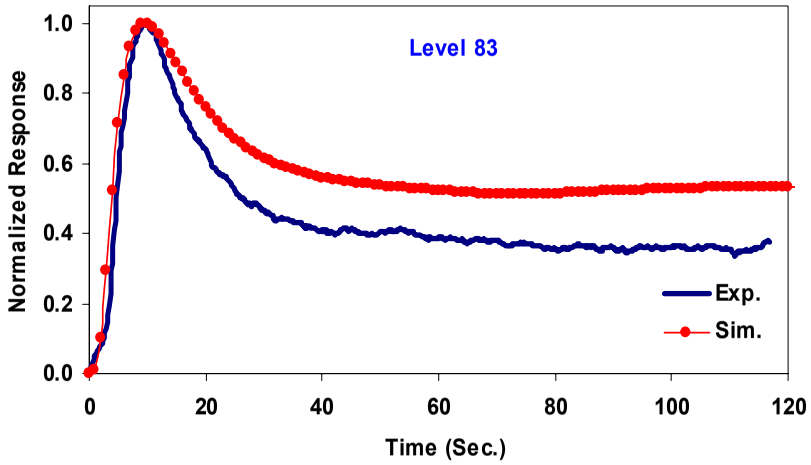

(c)

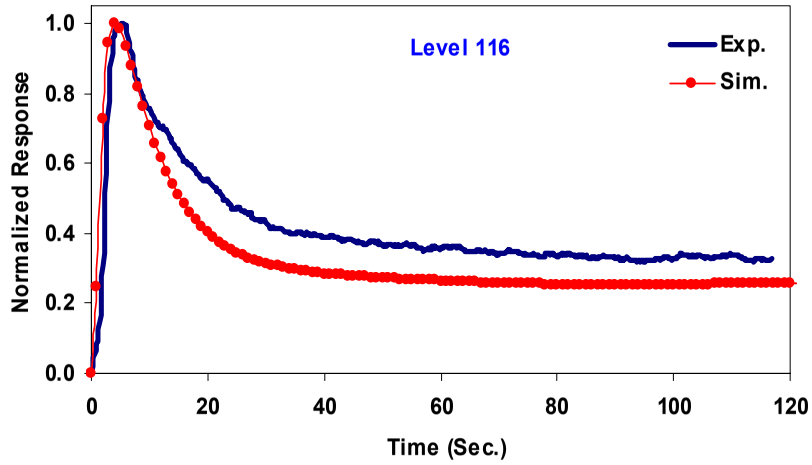

(d)

Figure 3 Comparison of Experimental and Simulated Tracer Responses for Run 16.7 (Tracer: - Catalyst; Injection Pt.: - Sidewall-Middle)`

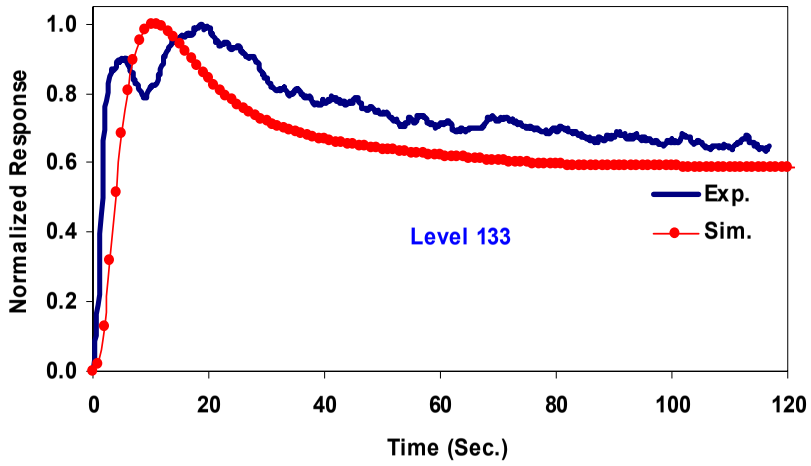

(e)

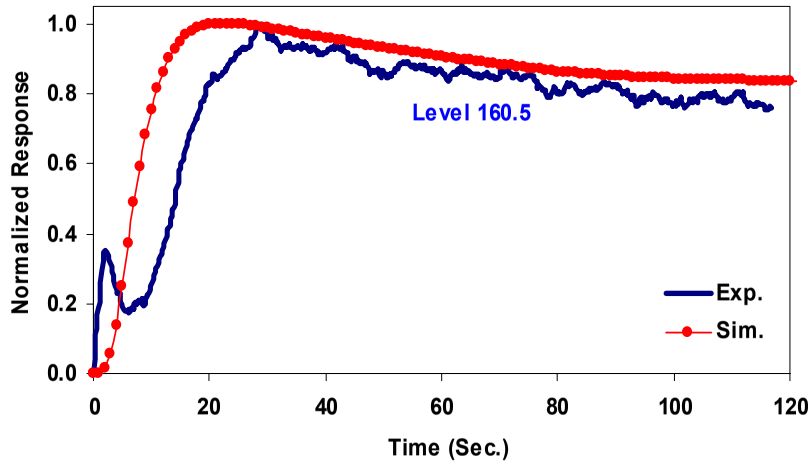

(f)

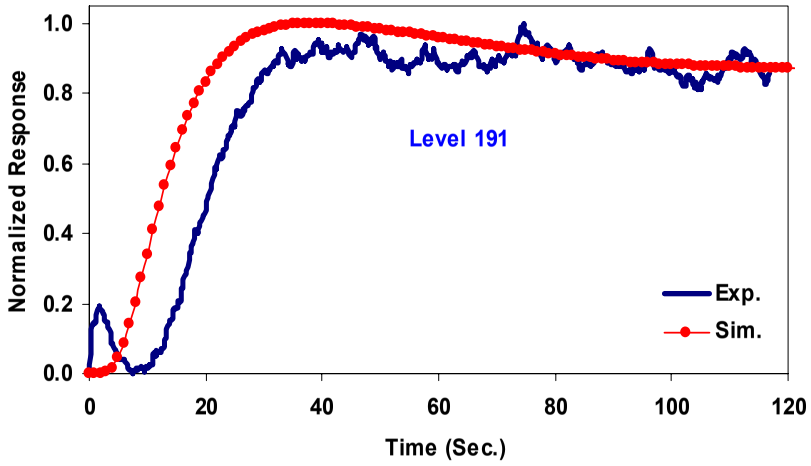

(g)

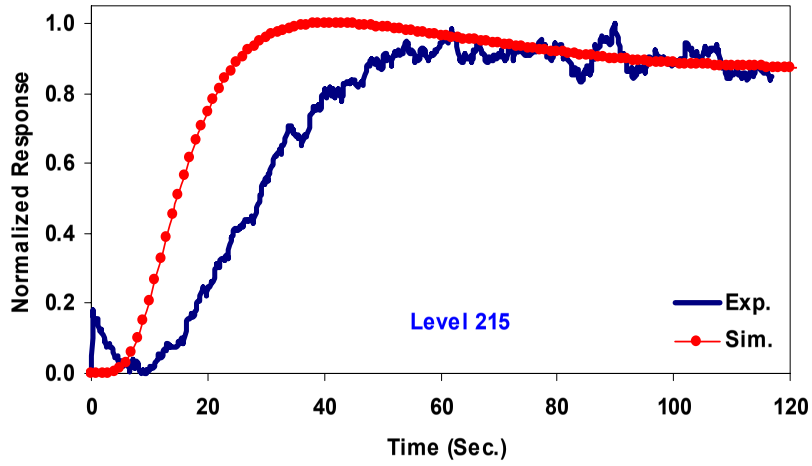

(h)

Figure 3 (continued) Comparison of Experimental and Simulated Tracer Responses for Run 16.7 (Tracer: - Catalyst; Injection Pt.: - Sidewall-Middle)

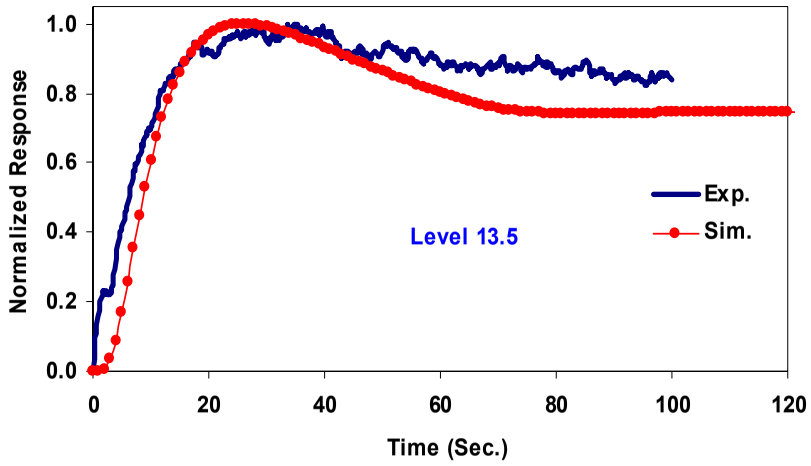

(a)

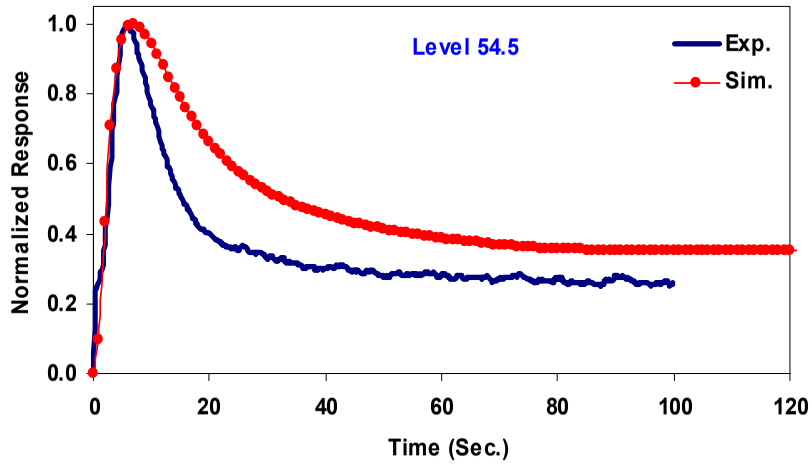

(b)

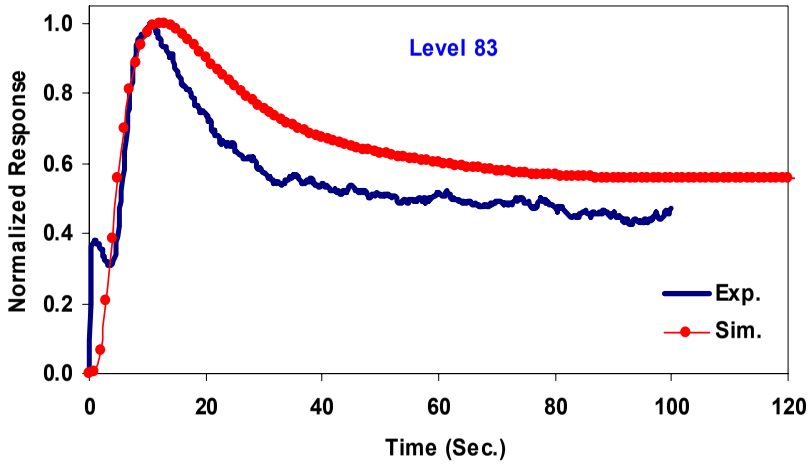

(c)

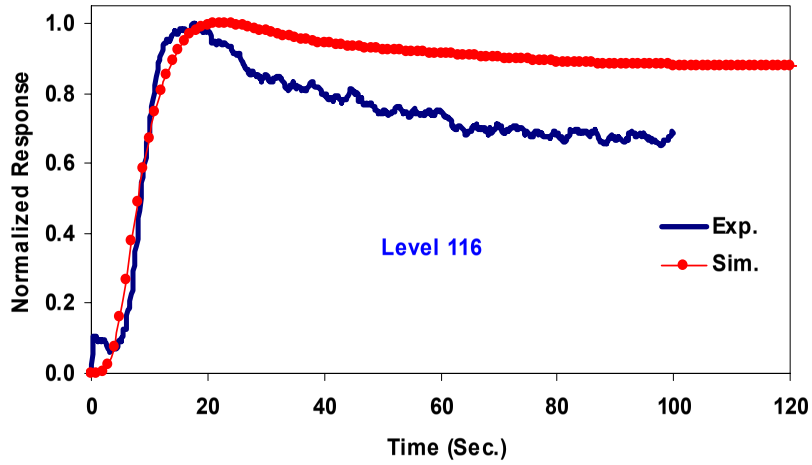

(d)

Figure 4 Comparison of Experimental and Simulated Tracer Responses for Run 16.7 (Tracer: - Catalyst; Injection Pt.: - Center-Bottom)

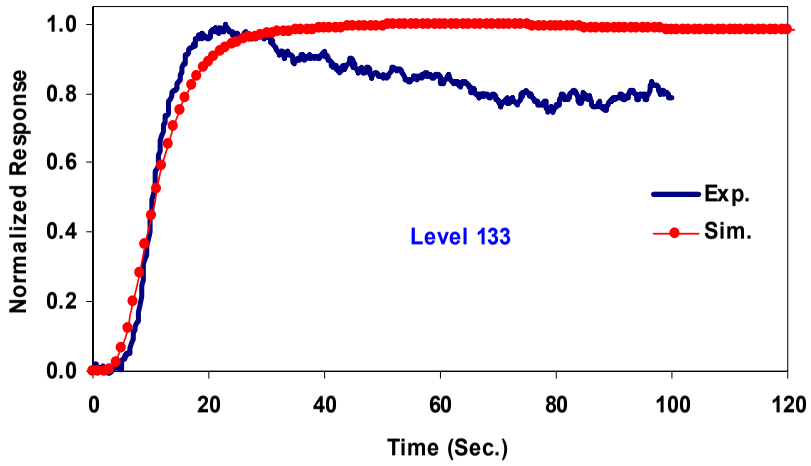

(e)

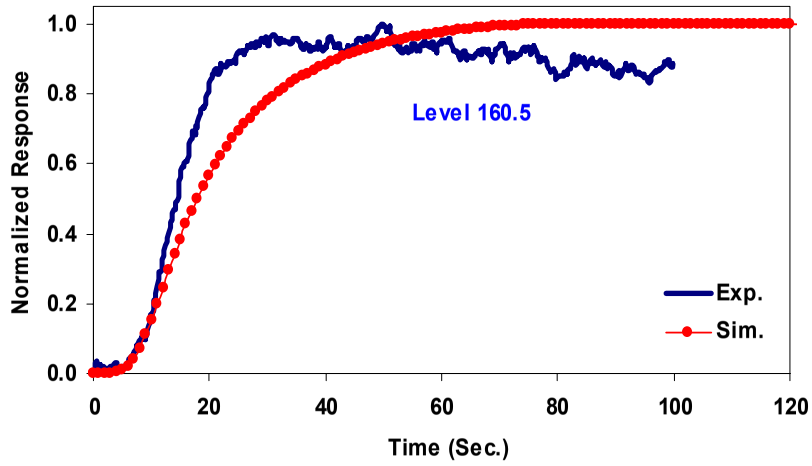

(f)

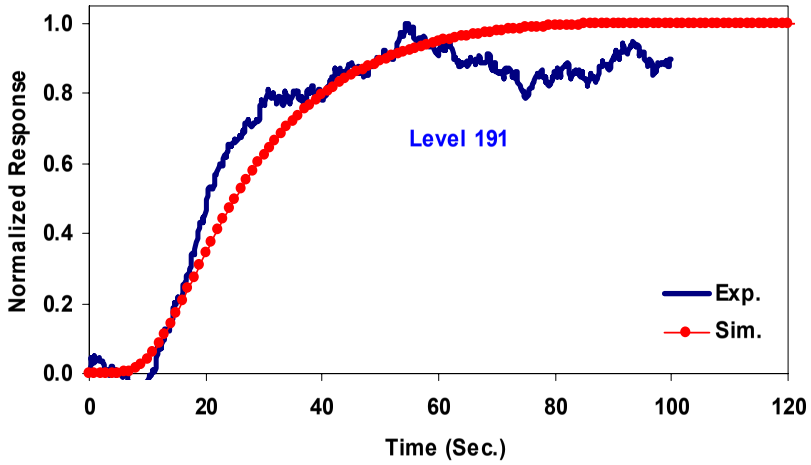

(g)

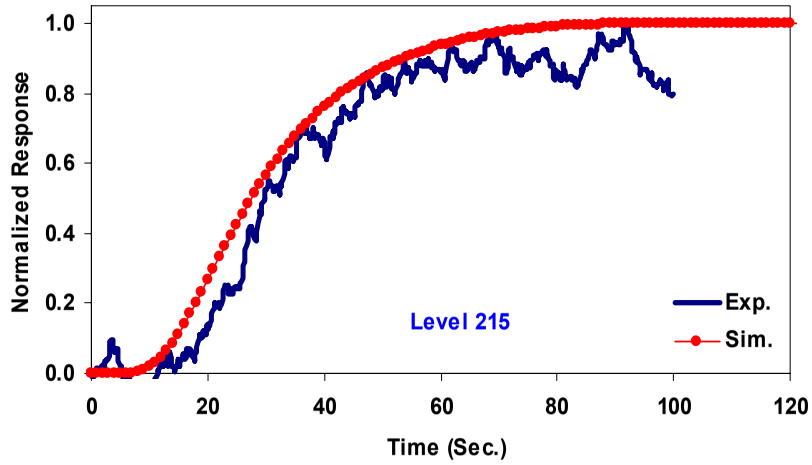

(h)

Figure 4 (continued) Comparison of Experimental and Simulated Tracer Responses for Run 16.7 (Tracer: - Catalyst; Injection Pt.: - Center-Bottom)

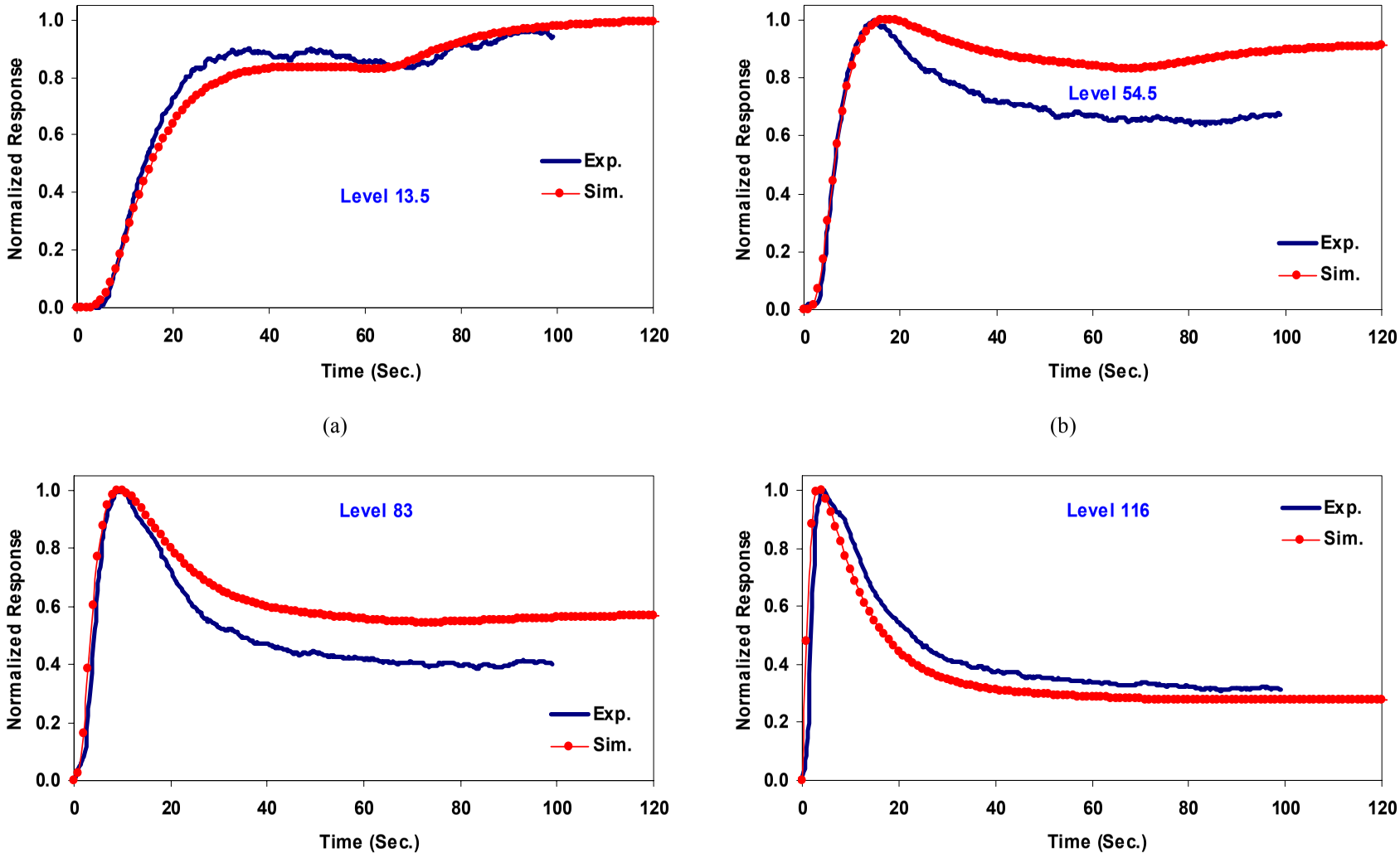

Figure 5 Comparison of Experimental and Simulated Tracer Responses for Run 16.7 (Tracer: - Mn_2O_3; Injection Pt.: - Sidewall-Middle)

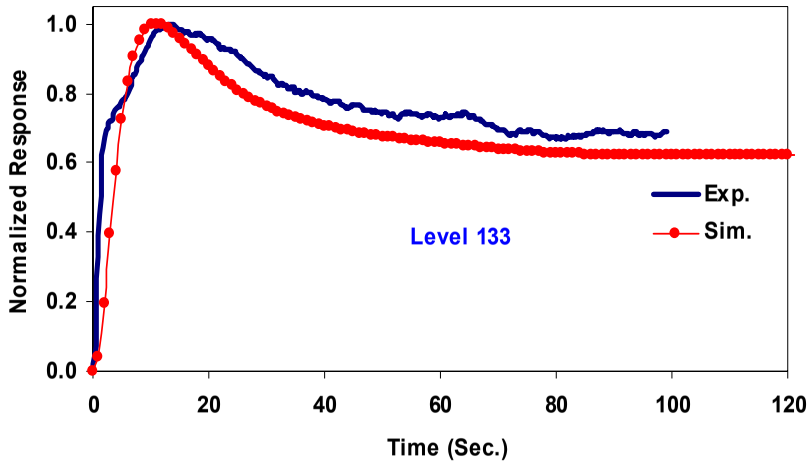

(e)

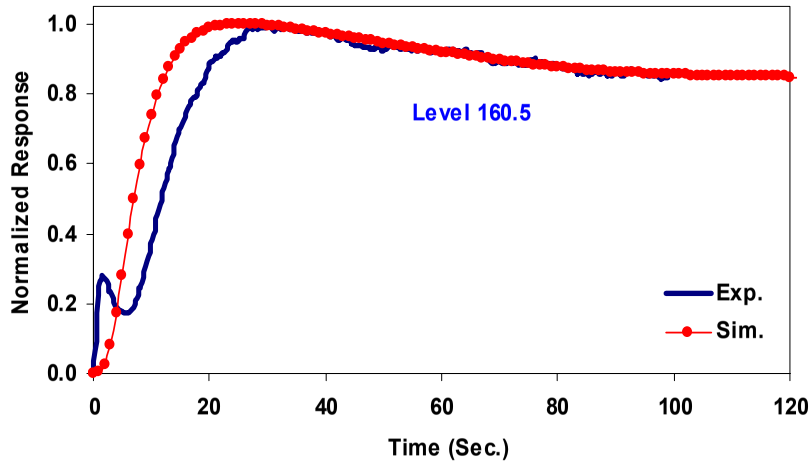

(f)

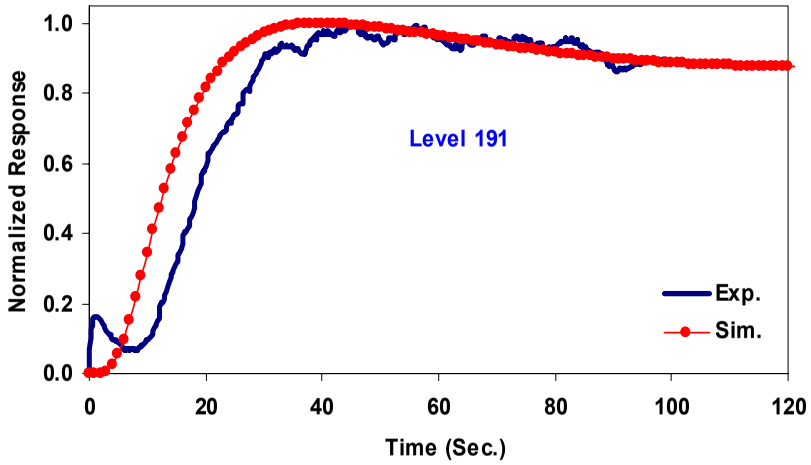

(g)

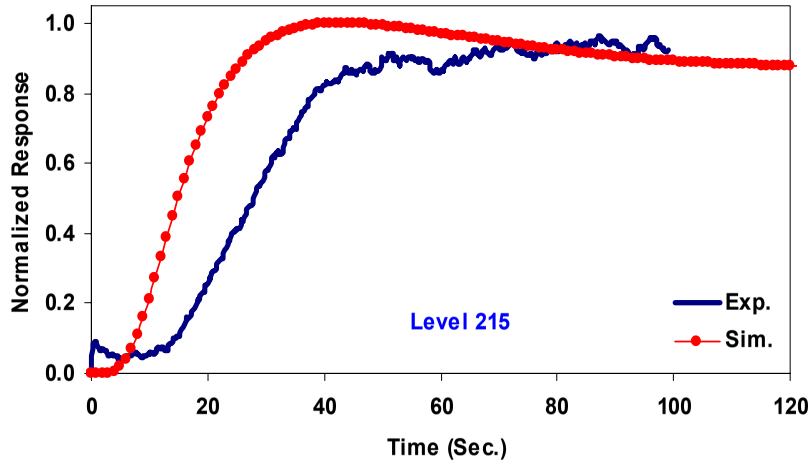

(h)

Figure 5 (continued) Comparison of Experimental and Simulated Tracer Responses for Run 16.7 (Tracer: - Mn_2O_3; Injection Pt.: - Sidewall-Middle)

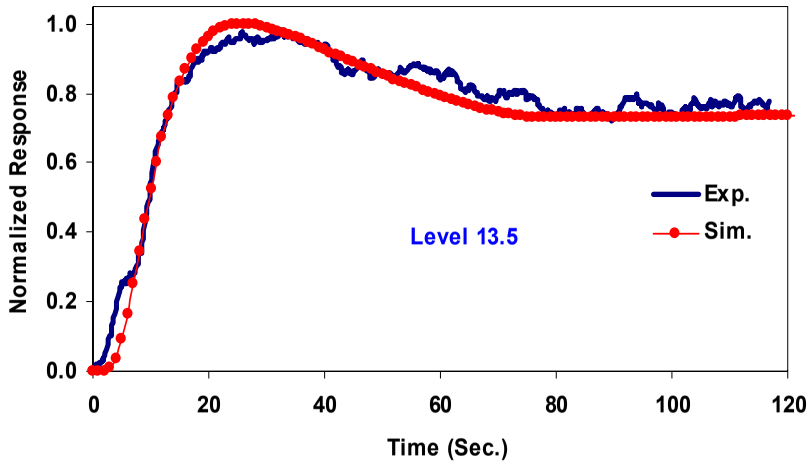

(a)

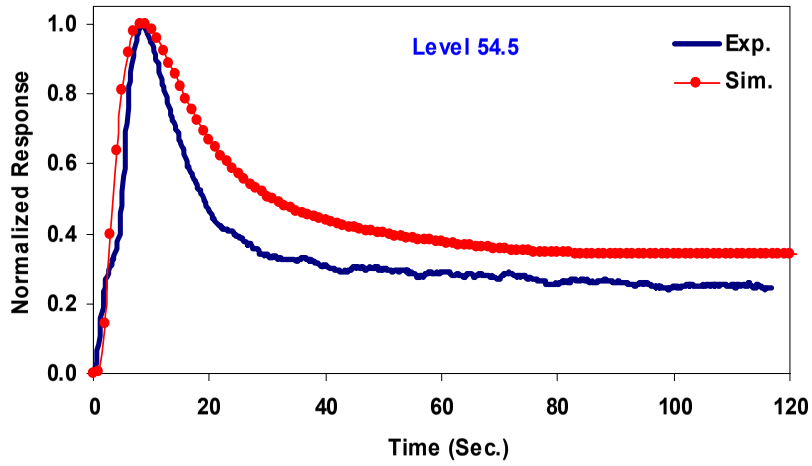

(b)

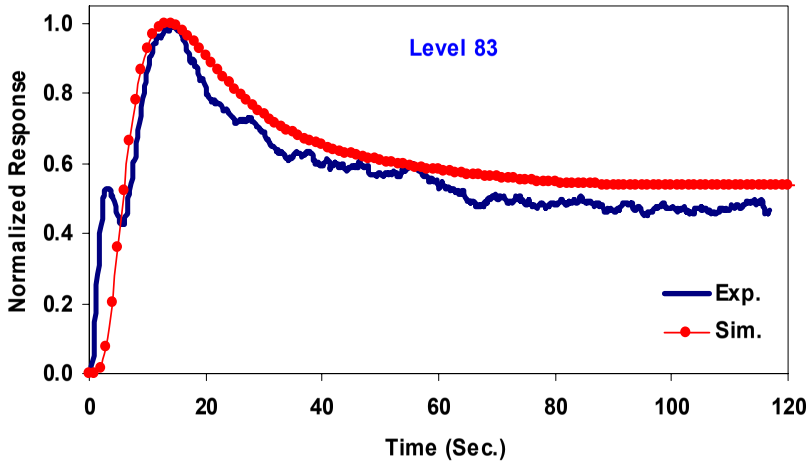

(c)

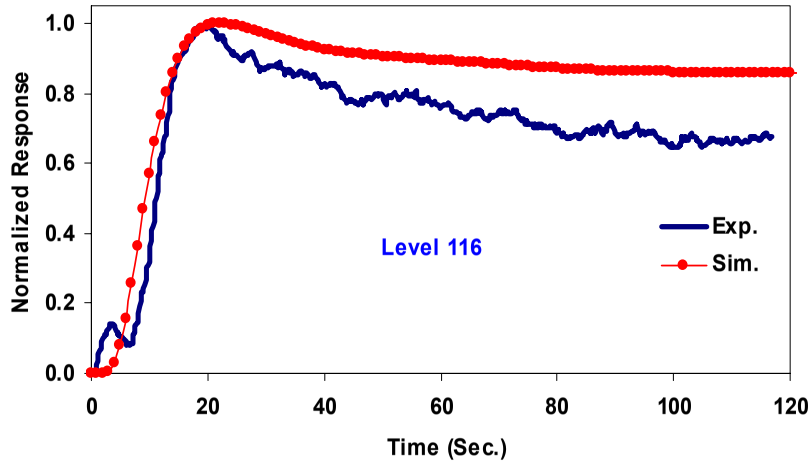

(d)

Figure 6 Comparison of Experimental and Simulated Tracer Responses for Run 16.7 (Tracer: - Mn_2O_3; Injection Pt.: - Center-Bottom)

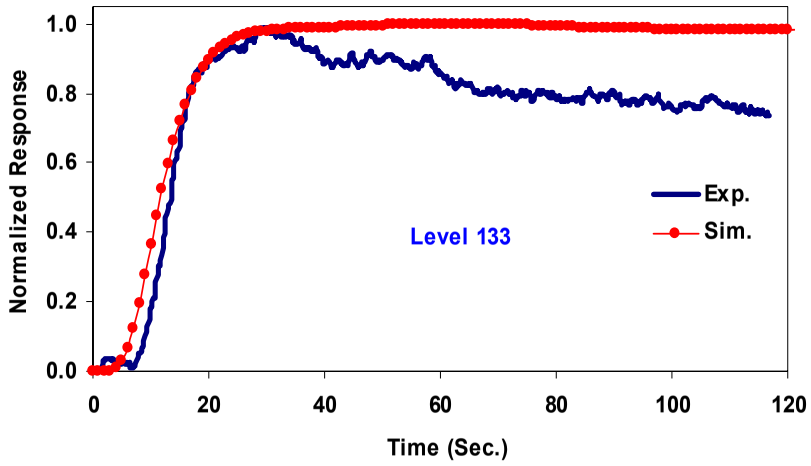

(e)

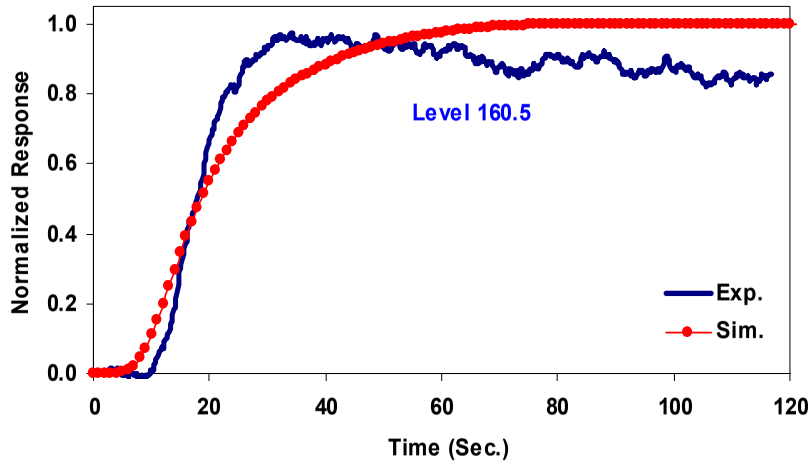

(f)

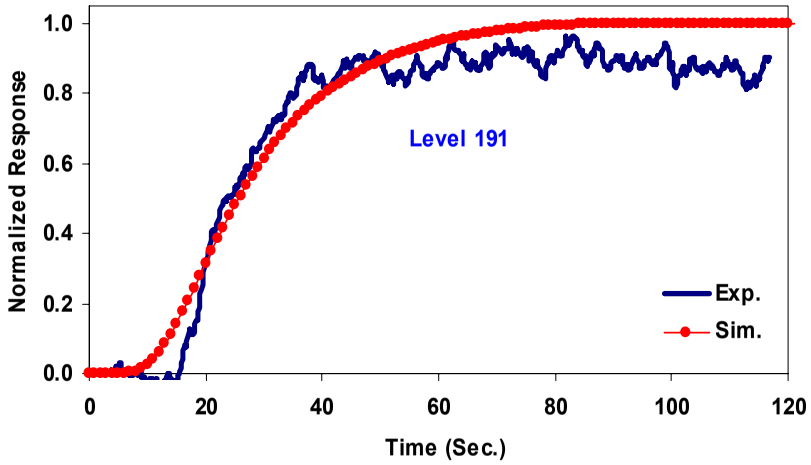

(g)

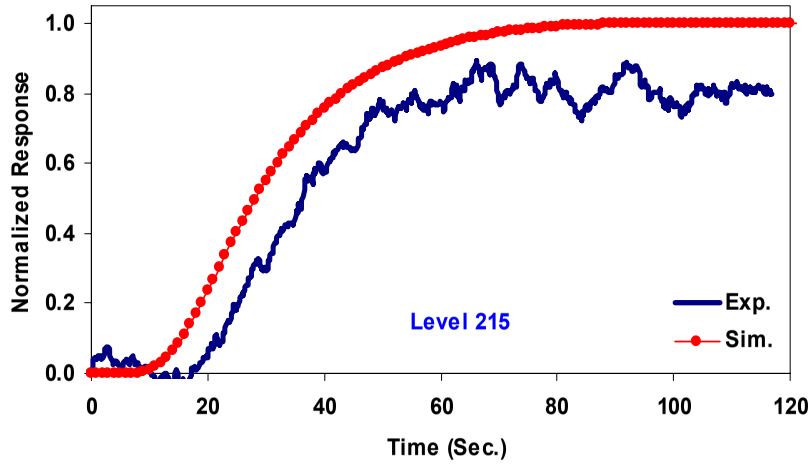

(h)

Figure 6 (continued) Comparison of Experimental and Simulated Tracer Responses for Run 16.7 (Tracer: - Mn_2O_3; Injection Pt.: - Center-Bottom)

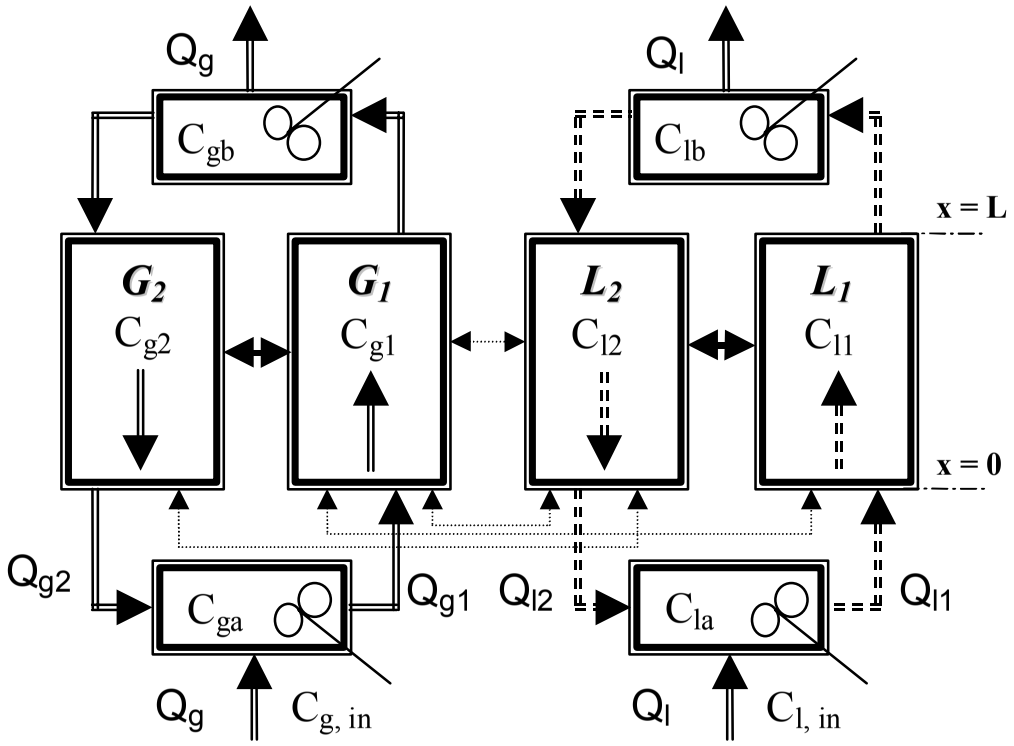

Figure 7 Schematic of the Reactor Compartmentalization for the Gas-Liquid Mixing Model with Interphase Mass Transfer

Table 2 Model Equations for Single Bubble Class Gas-Liquid Recirculation Model

$$\frac{\partial C_{g1}}{\partial t} = \left\{ \overline{D}_{xx_1} \frac{\partial^2 C_{g1}}{\partial x^2} - \overline{u}_{g1} \frac{\partial C_{g1}}{\partial x} - \frac{4\left(\overline{D}_{rr}\varepsilon_g\right)_{r=r''}}{r'' R\,\overline{\varepsilon}_{g1}}\left(C_{g1} - C_{g2}\right) + R_{x,g1} - \frac{k_{gulu}a_{gulu}}{\overline{\varepsilon}_{g1}}\left(HC_{g1} - C_{l1}\right) - \frac{k_{guld}a_{guld}}{\overline{\varepsilon}_{g1}}\left(HC_{g1} - C_{l2}\right) \right\}$$

$$\frac{\partial C_{g2}}{\partial t} = \left\{ \overline{D}_{xx_2} \frac{\partial^2 C_{g2}}{\partial x^2} + \overline{u}_{g2} \frac{\partial C_{g2}}{\partial x} - \frac{k_{gdld}a_{gdld}}{\overline{\varepsilon}_{g2}}\left(HC_{g2} - C_{l2}\right) + \frac{4r''/R}{R^2 - r''^2}\frac{\left(\overline{D}_{rr}\varepsilon_g\right)_{r=r''}}{\overline{\varepsilon}_{g2}}\left(C_{g1} - C_{g2}\right) + R_{x,g2} \right\}$$

$$\frac{\partial C_{l1}}{\partial t} = \left\{ \overline{D}_{xx_1} \frac{\partial^2 C_{l1}}{\partial x^2} - \overline{u}_{l1} \frac{\partial C_{l1}}{\partial x} + \left(\frac{r''}{r'}\right)^2 \frac{k_{gulu}a_{gulu}}{\overline{\varepsilon}_{l1}}\left(HC_{g1} - C_{l1}\right) - \frac{4\left(\overline{D}_{rr}\varepsilon_l\right)_{r=r'}}{r' R\,\overline{\varepsilon}_{l1}}\left(C_{l1} - C_{l2}\right) + R_{x,l1} \right\}$$

$$\frac{\partial C_{l2}}{\partial t} = \left\{ \overline{D}_{xx_2} \frac{\partial^2 C_{l2}}{\partial x^2} + \overline{u}_{l2} \frac{\partial C_{l2}}{\partial x} + \frac{4r'/R}{R^2 - r'^2}\frac{\left(\overline{D}_{rr}\varepsilon_l\right)_{r=r'}}{\overline{\varepsilon}_{l2}}\left(C_{l1} - C_{l2}\right) + \left(\frac{r''^2}{R^2 - r'^2}\right)\frac{k_{guld}a_{guld}}{\overline{\varepsilon}_{l2}}\left(HC_{g1} - C_{l2}\right) + R_{x,l2} + \left(\frac{R^2 - r''^2}{R^2 - r'^2}\right)\frac{k_{gdld}a_{gdld}}{\overline{\varepsilon}_{l2}}\left(HC_{g2} - C_{l2}\right) \right\}$$

$$\frac{dC_{ga}}{dt} = \left\{ \frac{\overline{\varepsilon}_{g2}\overline{u}_{g2}}{\overline{\varepsilon}_g \phi_{in} D_C}\frac{\left(R^2 - r''^2\right)}{R^2}C_{g2,0} - \frac{\overline{\varepsilon}_{g1}\overline{u}_{g1}}{\overline{\varepsilon}_g \phi_{in} D_C}\frac{r''^2}{R^2}C_{ga} + \frac{U_G}{\overline{\varepsilon}_g \phi_{in} D_C}C_{g,in} - \frac{k_{CST}a_{CST}}{\overline{\varepsilon}_g}\left(HC_{ga} - C_{la}\right) + R_{x,ga} \right\}$$

$$\frac{dC_{la}}{dt} = \left\{ \frac{\overline{\varepsilon}_{l2}\overline{u}_{l2}}{\overline{\varepsilon}_l \phi_{in} D_C}\frac{\left(R^2 - r'^2\right)}{R^2}C_{l2,0} - \frac{\overline{\varepsilon}_{l1}\overline{u}_{l1}}{\overline{\varepsilon}_l \phi_{in} D_C}\frac{r'^2}{R^2}C_{la} + \frac{U_L}{\overline{\varepsilon}_l \phi_{in} D_C}C_{l,in} + \frac{k_{CST}a_{CST}}{\overline{\varepsilon}_l}\left(HC_{ga} - C_{la}\right) + R_{x,la} \right\}$$

$$\frac{dC_{gb}}{dt} = \left\{ \frac{\overline{\varepsilon}_{g1}\overline{u}_{g1}}{\overline{\varepsilon}_g \phi_{out} D_C}\frac{r''^2}{R^2}C_{g1,L} - \frac{\overline{\varepsilon}_{g2}\overline{u}_{g2}}{\overline{\varepsilon}_g \phi_{out} D_C}\frac{\left(R^2 - r''^2\right)}{R^2}C_{gb} - \frac{U_G}{\overline{\varepsilon}_g \phi_{out} D_C}C_{gb} - \frac{k_{CST}a_{CST}}{\overline{\varepsilon}_g}\left(HC_{gb} - C_{lb}\right) + R_{x,gb} \right\}$$

$$\frac{dC_{lb}}{dt} = \left\{ \frac{\overline{\varepsilon}_{l1}\overline{u}_{l1}}{\overline{\varepsilon}_l \phi_{out} D_C}\frac{r'^2}{R^2}C_{l1,L} - \frac{\overline{\varepsilon}_{l2}\overline{u}_{l2}}{\overline{\varepsilon}_l \phi_{out} D_C}\frac{\left(R^2 - r'^2\right)}{R^2}C_{lb} - \frac{U_L}{\overline{\varepsilon}_l \phi_{out} D_C}C_{lb} + \frac{k_{CST}a_{CST}}{\overline{\varepsilon}_l}\left(HC_{gb} - C_{lb}\right) + R_{x,lb} \right\}$$

$$d_B = \overline{d}_B$$

Hydrodynamic Model

$$\varepsilon_g(\xi) = \overline{\varepsilon}_g \left(\frac{m+2}{m+2-2c}\right)\left(1 - c\xi^m\right)$$

Liquid Phase	Gas Phase
$0 = -\left(\rho_g \varepsilon_g + \rho_l \varepsilon_l\right) g - \frac{dP}{dz} + \frac{1}{r}\frac{d}{dr}\left(r\varepsilon_l \left\{ \overbrace{\tau^m_{l,rz} + \tau^t_{l,rz}}^{\tau_{l,rz}} \right\} \right)$	$0 = -\rho_g \varepsilon_g g - \varepsilon_g \frac{dP}{dz} + M_d$
$\tau_{l,rz}(\xi) = -\frac{\rho_l \nu_l^m}{R}\frac{du_l}{d\xi} - \frac{\rho_l l^2}{R^2}\left(\frac{du_l}{d\xi}\right)^2$	$M_d = -\frac{3\varepsilon_l \varepsilon_g \rho_l C_D}{4 d_B}\left(u_l - u_g\right)^2$
$\frac{l(\xi)}{R} = \frac{a(1-\xi)}{(\xi+b)^c} + d(1-\xi)^e$ Kumar *et al.* (1995)	$C_D = max\left[\frac{24}{Re}\left(1 + 0.15\,Re^{0.687}\right), \frac{8}{3}\frac{Eo}{Eo+4}\right]$ Tomiyama *et al.* (1995)

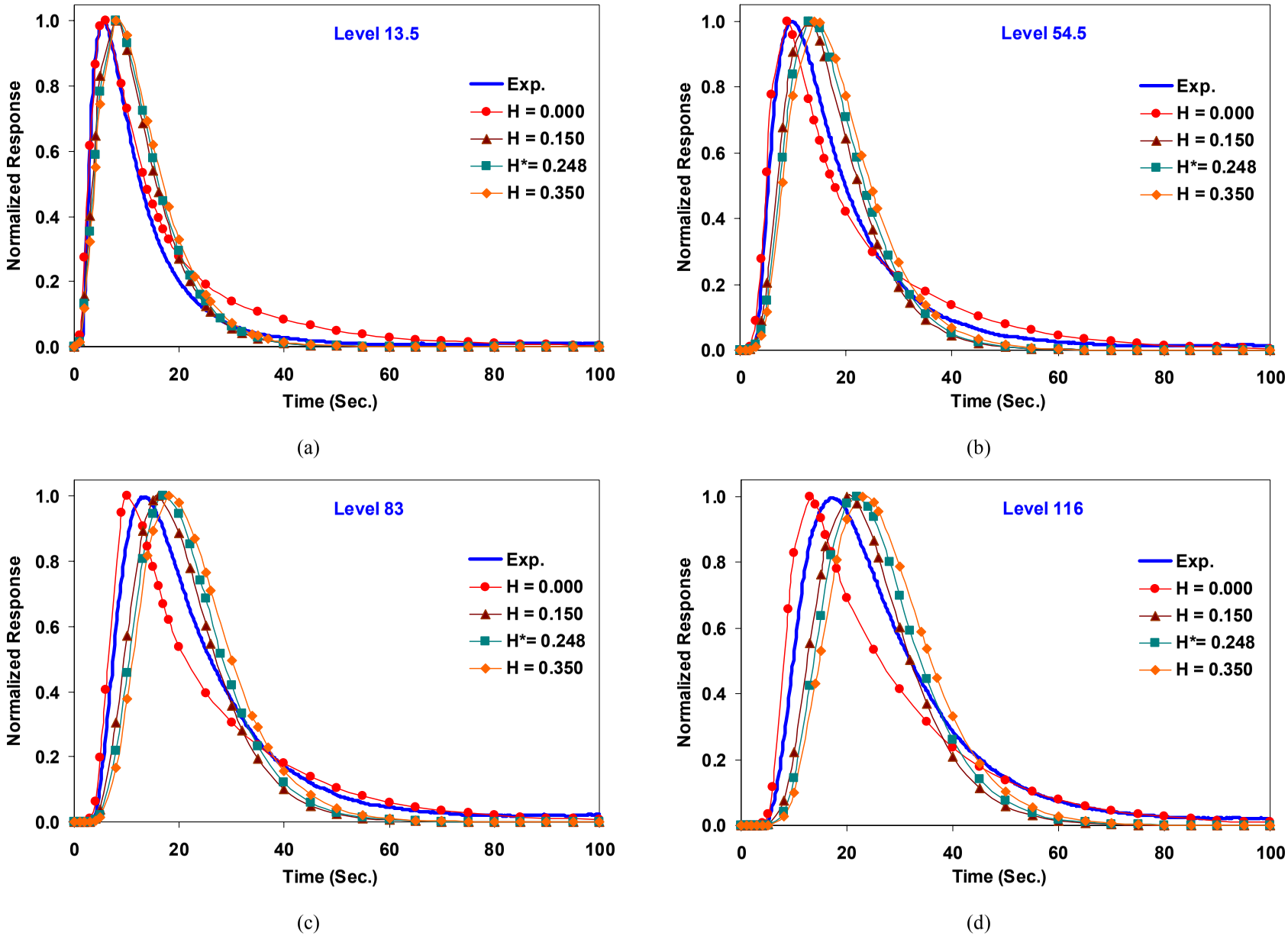

Figure 8 Comparison of Experimental and Simulated Gas Tracer Response Curves for Run 16.6 for Different Henry's Constants

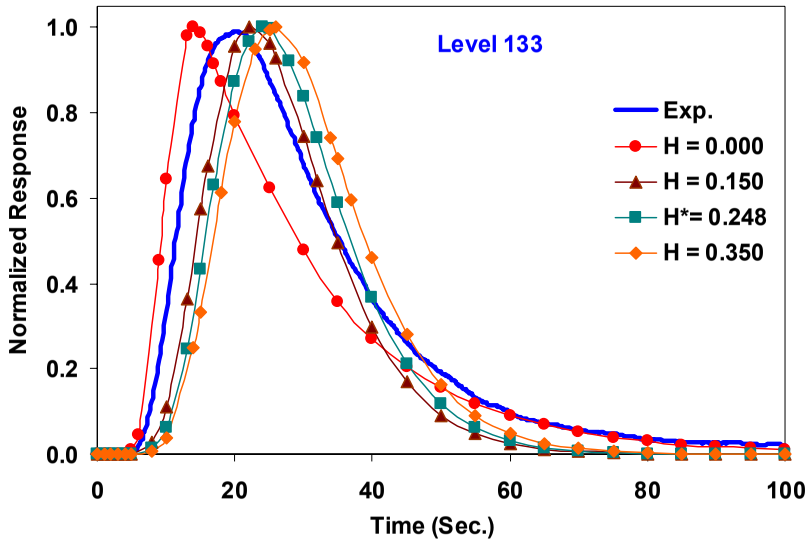

(e)

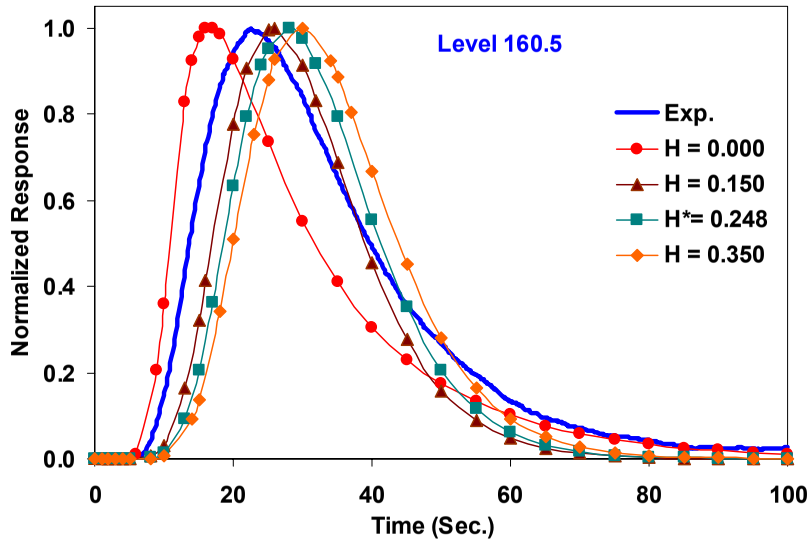

(f)

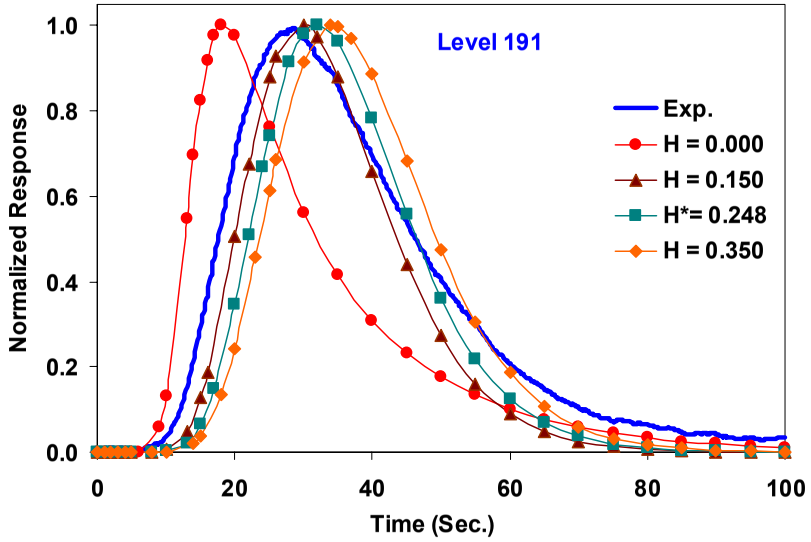

(g)

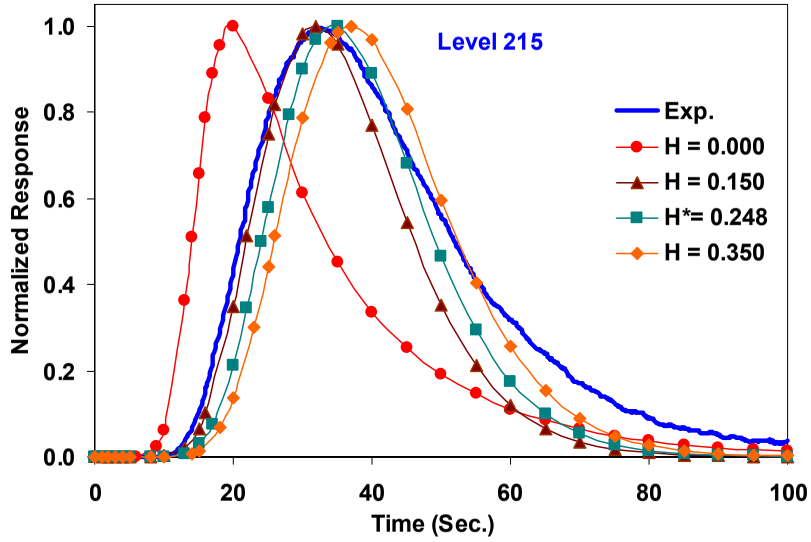

(h)

Figure 8 (continued) Comparison of Experimental and Simulated Gas Tracer Response Curves for Run 16.6 for Different Henry's Constants

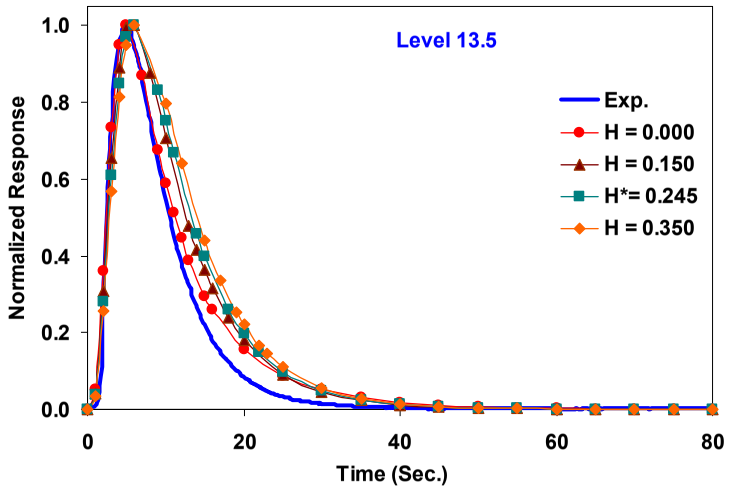

(a)

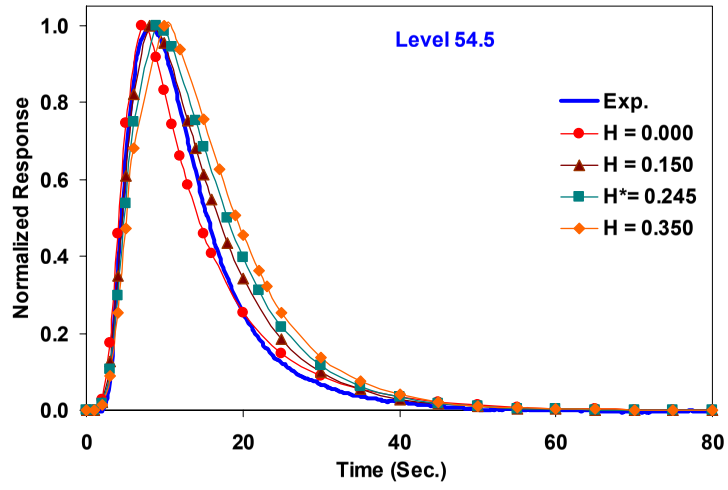

(b)

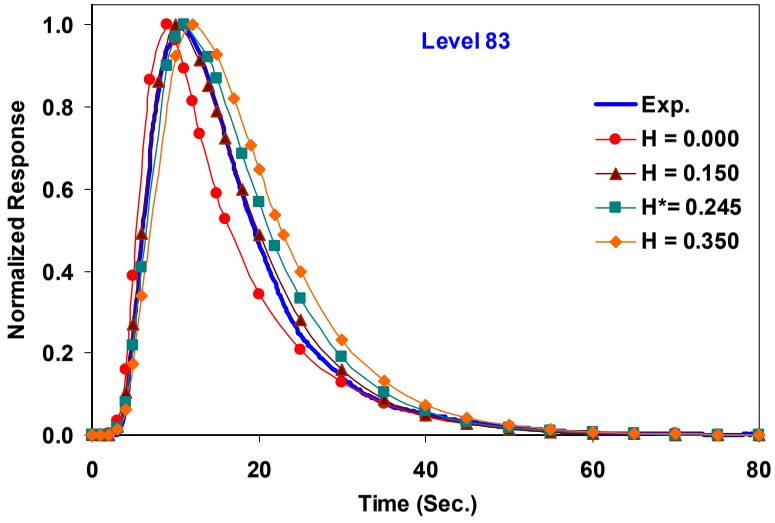

(c)

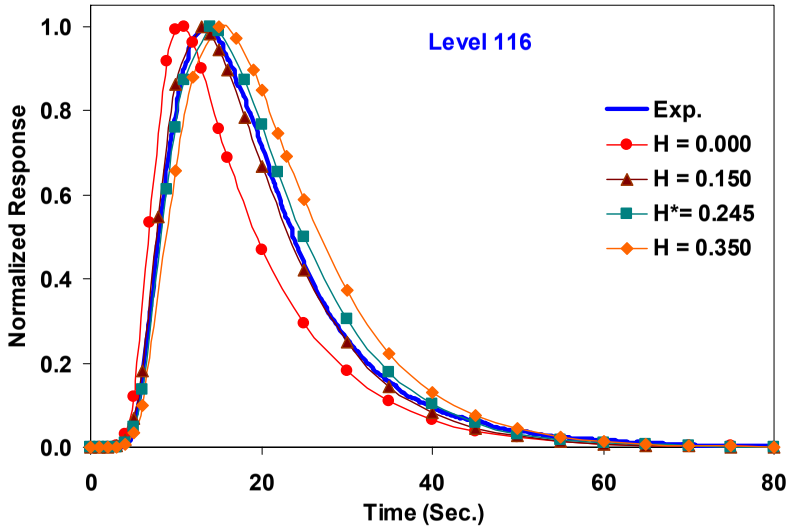

(d)

Figure 9 Comparison of Experimental and Simulated Gas Tracer Response Curves for Run 16.7 for Different Henry's Constants

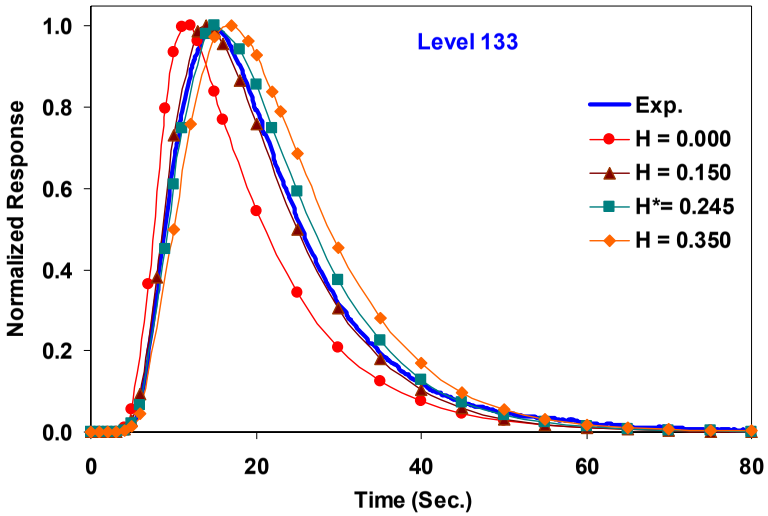

(e)

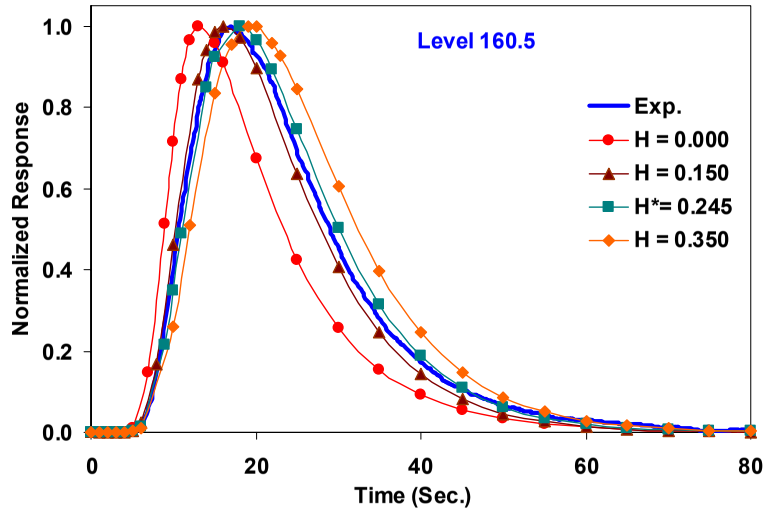

(f)

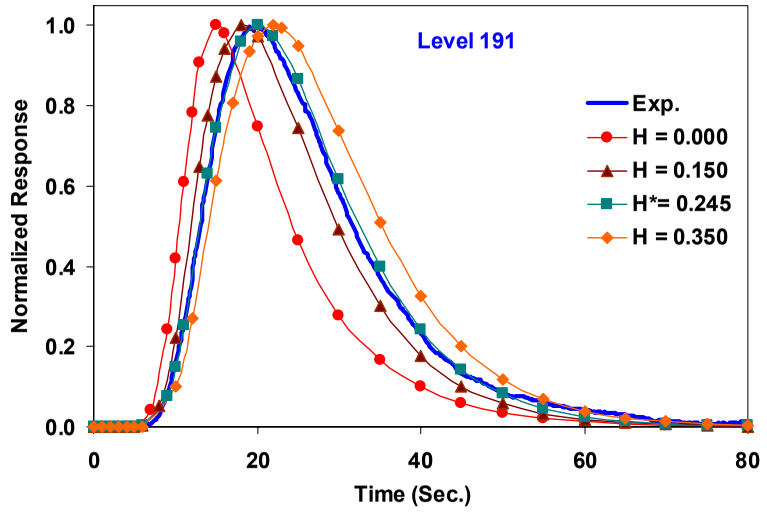

(g)

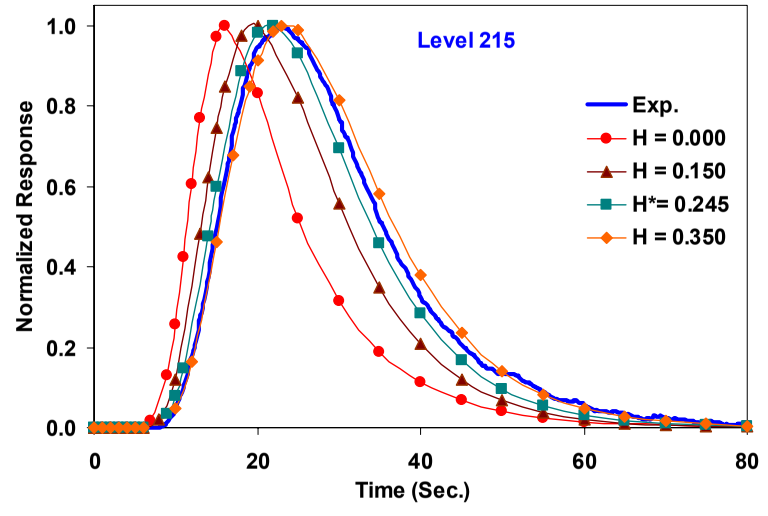

(h)

Figure 9 (continued) Comparison of Experimental and Simulated Gas Tracer Response Curves for Run 16.7 for Different Henry's Constants